



UNIVERSITAT
POLITÈCNICA
DE VALÈNCIA



ESCUELA TÉCNICA
SUPERIOR INGENIERÍA
INDUSTRIAL VALENCIA

CHEMICAL ENGINEERING MASTER THESIS

STUDY OF RADICAL CHEMISTRY IN ADVANCED OXIDATION PROCESSES BASED ON ULTRASOUND RADIATION IN WATER FOR PHARMACEUTICAL DRUGS REMOVAL

AUTHOR: Thibault Dewitte

SUPERVISOR: Javier José Navarro Laboulais

SUPERVISOR: Ricardo Antonio Torres-Palma

Academic year: 2020-21

Welcome to chemical kinetics haha! ~ J. Navarro

THANKINGS

Here I am. On a rooftop terrace in Palermo, doing the final checks and writing the last words of my final work for obtaining a master's degree in industrial engineering, chemistry. A final work or thesis that was made in an exceptional way. On the one hand because of the Covid pandemic that has been in jeopardy for almost two years and on the other hand was completed at the polytechnic university of Valencia (UPV) as part of an Erasmus exchange. A thesis that showed me the completely different side of science and that gave me a great research experience.

First of all, I would like to thank all the people who made this exchange possible for me during this difficult period. All the people of the international service at the KU Leuven and the UPV a big thank you! Secondly, I would like to thank my parents, who have given me all the support in every way to drag me through this adventure. Thank you for giving me the confidence to find my own way in a place more than a thousand kilometers away. Thirdly, I would like to thank my dearest friend, my girlfriend Ambroos. My support that assisted me all this time via video chat and telephone contact when I was struggling and who gave me the opportunity to see the world in a different way. Even now, when I do the last *fine tunings* on my thesis during our travel, you understand me, thank you! Fourthly, I would like to thank my second promotor professor Riccardo A. Torres-Palma and PhD Efraim Serna-Galvis for the collaboration and providing us the necessary data for calibration of the model.

And of course, finally, I would like to thank the best thesis promoter of ETSII. Professor Navarro, or "just Javier." Thank you for the huge opportunity you gave me. To immerse myself in a completely unprecedented world (for me anyway) of chemical computer technology and kinetic studies. To give me the confidence and motivate me during our cooperation. I hope that my final work can therefore be of effective use in the near future, and if so, I owe it to you. I hope to see you again in the future and then without distance and face mask rules. I will never forget you, and I hope you will never forget me as well.

Mom, Dad, Ambroos, Javier and all my friends who have supported me, thank you for everything!

Now, I am ready to jump into the real world and using my knowledge obtained over the past five years to help the world to be a better place.

DANKWOORD

Hier zit ik dan. Op een dakterras in Palermo doe ik de laatste controles en schrijf ik de laatste woordjes aan mijn eindproef voor het behalen van een master industriële ingenieurswetenschappen, chemie. Een eindproef of thesis die werd gemaakt op een uitzonderlijke manier. Enerzijds door de Covid pandemie die ons allen al bijna twee jaar in gedrang houdt en anderzijds werd afgerond aan de polytechnische universiteit van Valencia (UPV) in het kader van een Erasmus uitwisseling. Een thesis die mij de compleet andere kant van de wetenschap liet zien en die mij een geweldige onderzoekservaring gaf.

Eerst en vooral wil ik van harte alle mensen bedanken die mij deze uitwisseling mogelijk maakten in deze moeilijke periode. Alle mensen van de internationale dienst op de KU Leuven en de UPV een dikke merci! Ten tweede wil ik mijn ouders bedanken, die mij alle steun gegeven hebben op alle manieren om mij doorheen dit avontuur te sleuren. Bedankt om mij dan ook het vertrouwen te geven mijn eigen weg te vinden op een plek meer dan duizend kilometer van jullie verwijderd. Ten derde dank ik graag mijn allerliefste vriendin Ambroos. Mijn steun en toeverlaat die me al die tijd via videochat en telefonisch contact bijstond toen ik het moeilijk had en die mij de kans gaf om de wereld te zien op een andere manier. Ook nu nog, wanneer ik op reis de laatste *finetuning* doe aan mijn thesis begrijp je me, dankjewel! Ten vierde wil ik ook mijn tweede promotor prof Ricardo A. Torres-Palma en PhD Efraim A. Serna-Galvis bedanken voor de samenwerking en het verzorgen van de data nodig om ons model te kalibreren.

En natuurlijk als laatste wil ik de beste thesis promotor van ETSII bedanken. Professor Navarro, ofwel 'gewoon Javier'. Bedankt voor de enorme kans die je mij gaf. Om mij onder te dompelen in een compleet ongekende wereld (voor mij dan toch) van de chemische computertechnologie en de kinetische studies. Mij het vertrouwen te geven en mij te motiveren tijdens onze samenwerking. Ik hoop dat mijn eindwerk dan ook effectief van nut kan zijn in de nabije toekomst en als dat zo is, dan heb ik dit aan u te danken. Ik hoop je dan ook in de verdere toekomst en zonder afstand- en mondkapregels terug te zien. Ik zal u nooit vergeten en ik hoop jij mij ook niet.

Mama, papa, Ambroos, Javier en al mijn vrienden die mij hebben gesteund, bedankt voor alles!

Nu ben ik klaar om in de echte wereld te springen en mijn kennis van de afgelopen vijf jaar te gebruiken om de wereld te helpen een betere plek te zijn.

ABSTRACT

Because of a growing population and use of recalcitrant compounds (e.g. pharmaceuticals), advanced oxidation processes (AOP's) are a hot item in the last years of environmental research. One of these techniques is using ultrasonic waves to produce reactive species inside cavitation bubbles (acoustic cavitation) to react with recalcitrant components. In acoustic cavitation a lot of research is already done in the past, but in literature no model was introduced for the aqueous chemistry. This work includes a first approach for the reactions occurring in the aqueous phase when ultrasonic waves are irradiated in pure water and in presence of a pharmaceutical. Two models were created for sonochemistry in oxygen and air saturated (pure) water. The models were created by using the chemical simulation program KPP and with the use of Matlab codes the concentration profiles were obtained. The approach includes a source reaction term Φ that describes the production of radical species due to the acoustic cavitation. The model in air saturated water was calibrated for short sonication periods (20-30 minutes) in pure and pharmaceutical containing water and for longer sonication periods (2.5 hours) in only pure water. The outcome of the calibrations showed that the model works for short sonication periods. The calibration mostly was done by comparing the production of H_2O_2 in time experimentally and by simulation. For longer sonication periods, the resulting simulations still showed similar results, but concentration profiles were very different. Lastly, short time experiments with water containing a pharmaceutical compound (acetaminophen or ciprofloxacin) were carried out and compared with simulation results. When comparing these latter results, there are some discrepancies. This can be due to some missing effects or reactions in the model. This work can be an introduction for modelling acoustic cavitation but still more calibration experiments are needed to optimise the model.

Keywords: Ultrasounds, Pharmaceutical compounds removal, Chemical modelling, Advanced oxidation processes

RESUMEN

Debido a una creciente población y el uso de compuestos recalcitrantes a la descomposición (por ejemplo, productos farmacéuticos), los procesos de oxidación avanzada (AOP) son un tema candente en los últimos años de investigación ambiental. Una de estas técnicas es el uso de ondas ultrasónicas para producir especies reactivas dentro de burbujas de cavitación (cavitación acústica) que reaccionen con los componentes recalcitrantes. El campo de investigación en cavitación ultrasónica es muy antiguo, pero no hay un modelo estándar para las reacciones químicas que tienen lugar en fase acuosa. Este trabajo incluye un primer enfoque para las reacciones químicas que ocurren cuando las ondas ultrasónicas se irradian en agua pura y en presencia de un producto farmacéutico. Se crearon dos modelos sonoquímicos para el agua saturada en oxígeno y aire. Los modelos se crearon utilizando el programa de simulación química KPP y con el uso de códigos Matlab se obtuvieron los perfiles de concentración. El enfoque presentado en este trabajo incluye un término fuente de reacción que describe la producción de especies radicales debido a la cavitación acústica. El modelo en agua saturada de aire se calibró para períodos cortos de sonicación (20-30 minutos) tanto para agua pura como agua conteniendo productos farmacéuticos así como para períodos de sonicación más largos (2,5 horas) en agua pura. El resultado de las calibraciones mostró que el modelo funciona durante períodos de sonicación cortos. La calibración se realizó principalmente mediante la comparación de la producción experimental de H_2O_2 y su simulación a lo largo del tiempo. Para períodos de sonicación más largos, las simulaciones resultantes todavía mostraron resultados similares, pero los perfiles de concentración fueron muy diferentes. Por último, se llevaron a cabo experimentos a corto plazo con agua que contenía un compuesto farmacéutico y se compararon con los resultados de la simulación. Al comparar estos últimos resultados, hay algunas discrepancias. Esto puede deberse a algunos efectos o reacciones que faltan en el modelo.

Palabras clave: Ultrasonidos, Eliminación de compuestos farmacéuticos, Aguas residuales, procesos avanzados de oxidación, modelización química

RESUM

A causa d'una creixent població i l'ús de compostos recalcitrants a la descomposició (per exemple, productes farmacèutics), els processos d'oxidació avançada (AOP) són un tema candent en els últims anys d'investigació ambiental. Una d'aquestes tècniques és l'ús d'ones ultrasòniques per produir espècies reactives dins de bombolles de cavitació (cavitació acústica) que reaccionin amb els components recalcitrants. El camp de recerca en cavitació ultrasònica és molt antic però no hi ha un model estàndard per a les reaccions químiques que tenen lloc en fase aquosa. Aquest treball inclou un primer enfocament per a les reaccions químiques que ocorren quan les ones ultrasòniques s'irradien en aigua pura i en presència d'un producte farmacèutic. Es van crear dos models sonoquímics per a l'aigua saturada en oxigen i aire. Els models es van crear utilitzant el programa de simulació química KPP i amb l'ús de codis Matlab es van obtenir els perfils de concentració. L'enfocament presentat en aquest treball inclou un terme font de reacció que descriu la producció d'espècies radicals a causa de la cavitació acústica. El model en aigua saturada d'aire es va calibrar per períodes curts de sonicació (20-30 minuts) tant per a aigua pura com aigua contenint productes farmacèutics així com per a períodes de sonicació més llargs (2,5 hores) en aigua pura. El resultat dels calibratges va mostrar que el model funciona durant períodes de sonicació curts. El calibratge es va realitzar principalment mitjançant la comparació de la producció experimental d'H₂O₂ i la seva simulació al llarg del temps. Per a períodes de sonicació més llargs, les simulacions resultants encara van mostrar resultats similars, però els perfils de concentració van ser molt diferents. Finalment, es van dur a terme experiments a curt termini amb aigua que contenia un compost farmacèutic i es van comparar amb els resultats de la simulació. A l'comparar aquests últims resultats, hi ha algunes discrepàncies. Això pot ser degut a alguns efectes o reaccions que falten en el model.

Paraules clau: Ultrasons, Eliminació de compostos farmacèutics, Aigües residuals, processos avançats d'oxidació, modelització química

SAMENVATTING

Door een groeiende populatie en het gebruik van persistente verbindingen (bijv. farmaceutica) zijn geavanceerde oxidatieprocessen (AOP's) een "hot item" in de laatste jaren van milieuonderzoek. Een van deze technieken is het gebruik van ultrasone golven om reactieve componenten te produceren in cavitatiebellen (akoestische cavitatie) om te reageren met persistente componenten. Binnen de akoestische cavitatie werd in het verleden al veel onderzoek gedaan, maar in de literatuur werd nog geen model geïntroduceerd voor de aquatische chemie. Dit werk omvat een eerste benadering voor de reacties die optreden in de waterfase wanneer ultrasone golven worden bestraald in zuiver water en in aanwezigheid van een farmaceutische component. Er zijn twee modellen ontwikkeld voor sonochemie in zuurstof en lucht verzadigd (zuiver) water. De modellen werden gemaakt met behulp van het chemisch simulatieprogramma KPP en met behulp van Matlab-codes werden de concentratieprofielen verkregen. De aanpak omvat een bronreactieterm Φ die de productie van reactieve componenten beschrijft als gevolg van de akoestische cavitatie. Het model in lucht verzadigd water werd gekalibreerd voor korte sonicatieperioden (20-30 minuten) in zuiver en farmaceutica bevattend water en voor langere sonicatieperioden (2,5 uur) in alleen zuiver water. Het resultaat van de kalibraties toonde aan dat het model werkt voor korte sonicatieperioden. De kalibratie werd meestal uitgevoerd door de productie van H_2O_2 experimenteel en door simulatie te vergelijken. Voor langere sonicatieperioden vertoonden de resulterende simulaties nog steeds vergelijkbare resultaten, maar concentratieprofielen waren zeer verschillend. Ten slotte werden experimenten uitgevoerd met water dat een farmaceutische bevat voor korte sonicatieperiodes, vergeleken met simulatieresultaten. Bij het vergelijken van deze laatste resultaten zijn er enkele discrepanties. Dit kan te wijten zijn aan enkele ontbrekende effecten of reacties in het model. Dit werk kan een introductie zijn voor het modelleren van de aquatische chemie in akoestische cavitatie maar er zijn nog meer kalibratie-experimenten nodig om het model te optimaliseren.

Sleutelwoorden: Ultrasound, farmaceutica verwijdering, Chemische modellering, Geavanceerde oxidatietechnieken

Table of content

| | |
|-------------------------------------------------------------|-------------|
| THANKINGS | III |
| DANKWOORD | IV |
| ABSTRACT | V |
| RESUMEN | VI |
| RESUM | VII |
| SAMENVATTING | VIII |
| LIST OF FIGURES | XI |
| LIST OF TABLES | XII |
| CHAPTER 1: INTRODUCTION | 1 |
| 1.1 GENERAL..... | 1 |
| 1.2 OVERVIEW..... | 3 |
| CHAPTER 2: LITERATURE REVIEW | 4 |
| 2.1 INTRODUCTION | 4 |
| 2.2 ACOUSTIC CAVITATION | 4 |
| 2.2.1 <i>General</i> | 4 |
| 2.2.2 <i>Bubble dynamics</i> | 6 |
| 2.2.2.1 Bubble radius | 6 |
| 2.2.2.2 Bubble temperature and pressure..... | 7 |
| 2.2.2.3 Number of bubbles | 8 |
| 2.2.3 <i>Chemical kinetics</i> | 9 |
| 2.2.3.1 Reactions inside or near the bubble | 9 |
| 2.2.3.2 Chemical kinetics | 11 |
| 2.3 OPERATIONAL PARAMETERS | 12 |
| 2.3.1 <i>Soundwave properties</i> | 12 |
| 2.3.2 <i>Dissolved gasses</i> | 13 |
| 2.3.3 <i>Dissolved ions</i> | 13 |
| 2.3.4 <i>Reaction time</i> | 14 |
| 2.3.5 <i>H₂O₂ concentration</i> | 14 |
| 2.4 REACTOR CONFIGURATIONS | 15 |
| 2.4.1 <i>Working principle of an US transducer</i> | 15 |
| 2.4.2 <i>Sonochemical horn</i> | 17 |
| 2.4.3 <i>Ultrasonic bath</i> | 17 |
| 2.4.4 <i>Multiple-frequency reactor</i> | 17 |
| 2.4.5 <i>Operating temperature and pressure</i> | 18 |
| 2.5 ULTRASONIC PHARMACEUTICAL REMOVAL..... | 19 |
| 2.6 OBJECTIVES..... | 20 |
| CHAPTER 3: MATERIALS AND METHODS | 21 |
| 3.1 INTRODUCTION | 21 |
| 3.2 THE KINETIC PRE-PROCESSOR (KPP) | 21 |
| 3.2.1 <i>Syntax rules</i> | 21 |
| 3.2.2 <i>Species file (Root.spc)</i> | 22 |
| 3.2.3 <i>Equation file (Root.eqn)</i> | 22 |
| 3.2.4 <i>Definition file (Root.def)</i> | 23 |
| 3.2.5 <i>Kpp file (Root.kpp)</i> | 25 |
| 3.2.6 <i>Numerical method</i> | 26 |
| 3.2.7 <i>Generated codes</i> | 27 |

| | | |
|---------------------------------------------------|---------------------------------------------------------------|-----------|
| 3.2.7.1 | Root_Main.m | 28 |
| 3.2.7.2 | Root_Fun.m | 28 |
| 3.2.7.3 | Root_Monitor.m | 28 |
| 3.2.7.4 | Root_Rates.m and Root_Update_RCONST.m | 28 |
| 3.2.7.5 | Root_Initialize.m | 28 |
| 3.3 | US EXPERIMENTS | 29 |
| 3.3.1 | <i>Reactor</i> | 29 |
| 3.3.2 | <i>Chemical analysis</i> | 30 |
| CHAPTER 4: CHEMICAL MODEL..... | | 31 |
| 4.1 | INTRODUCTION | 31 |
| 4.2 | MASS TRANSFER | 31 |
| 4.3 | PROPOSAL OF THE MODEL FOR US RADIATION IN WATER..... | 34 |
| 4.3.1 | <i>Based on Merouani</i> | 36 |
| 4.3.2 | <i>Based on Yasui</i> | 38 |
| 4.4 | EXTENSION OF THE MODEL – REACTIONS WITH PHARMACEUTICALS | 39 |
| CHAPTER 5: RESULTS AND DISCUSSION | | 41 |
| 5.1 | INTRODUCTION | 41 |
| 5.2 | MEROUANI MODEL | 41 |
| 5.3 | YASUI MODEL | 43 |
| 5.3.1 | <i>Short sonication times</i> | 43 |
| 5.3.2 | <i>Long sonication time (2.5 hours)</i> | 44 |
| 5.3.3 | <i>Sonication of water containing pharmaceuticals</i> | 47 |
| CHAPTER 6: CONCLUSION..... | | 50 |
| REFERENCES..... | | 53 |
| APPENDIX I: EXAMPLE EQUATION FILE..... | | 58 |
| APPENDIX II: EXAMPLE DEFINITION FILE | | 61 |
| APPENDIX III: EXAMPLE SPECIES FILE..... | | 63 |
| APPENDIX IV: EXAMPLE KPP FILE | | 64 |

List of figures

| | |
|------------------------------------------------------------------------------------------------------------------------------------------------------------------------------------------------------------------------------------------------------------------------------------------------------------------------------------------------------------------------------------------------------------------------------------------------------|----|
| FIGURE 1: AOP TECHNIQUES, ADAPTED FROM J. NAVARRO | 2 |
| FIGURE 2: COSTS OF AOP INVOLVING US FOR DYE REMOVAL, MAHAMUNI AND ADEWUYI (2010) | 3 |
| FIGURE 3: FORMATION AND COLLAPSE OF AN ACOUSTIC BUBBLE, CHATEL ET AL. (2015) | 4 |
| FIGURE 4: THE BUBBLE RADIUS OSCILLATION DUE TO AN ACOUSTIC PRESSURE WAVE, GE (2015) | 5 |
| FIGURE 5: FENTON REACTION PATHWAY IN ABCENSE OF ORGANICAL SUBSTANCES, FROM BARBUSINKI (2009)..... | 14 |
| FIGURE 6: PIEZOELECTRIC TRANSDUCER (SOURCE: HTTP://WWW.MRCOPHTH.COM/COMMONULTRASOUNDCASES/PRINCIPLESOFULTRASOUND.HTML) | 15 |
| FIGURE 7: STRUCTURE AND MOVEMENT OF A PIEZOELECTRIC MATERIAL, USED FROM HALAND (2017)..... | 16 |
| FIGURE 8: DIFFERENT WAYS OF ULTRASOUNDREACTORS, USED FROM C. GE (2015) | 17 |
| FIGURE 9: CONFIGURATION OF A MULTIPLE-FREQUENCY REACTOR, USED FROM GOGATE AND PATIL (2016)..... | 18 |
| FIGURE 10: THE EVOLUTION OF PUBLICATIONS ON AOP'S FOR PHARMACEUTICAL DEGRADATION (OBTAINED WITH DATA FROM SCOPUS, SEARCH: "AOPs AND PHARMACEUTICALS", ALL SUBJECTS) | 19 |
| FIGURE 11: SCHEME OF A SONOCHEMICAL BATCH REACTOR WITH COOLING JACKET, USED FROM MOUSALLY ET AL. (2019)..... | 20 |
| FIGURE 12: EXAMPLE OF THE CHEMICAL SPECIES FILE (ROOT.SPC) | 22 |
| FIGURE 13: EXAMPLE OF THE EQUATION FILE (ROOT.EQN) | 23 |
| FIGURE 14: CHEMICAL DESCRIPTION FILE EXAMPLE (ROOT.DEF)..... | 24 |
| FIGURE 15: INLINE CODES EXAMPLES IN THE DESCRIPTION FILE (ROOT.DEF) | 25 |
| FIGURE 16: ROOT.KPP FILE EXAMPLE | 25 |
| FIGURE 17: US REACTOR WITH COOLING JACKED, WITH PERMISSION OF E. SERNA-GALVIS..... | 29 |
| FIGURE 18: MASS TRANSFER OF A COMPONENT X FROM GAS TO LIQUID PHASE | 31 |
| FIGURE 19: NUMERICAL SIMULATIONS OF (LEFT) MEROUANI ET AL. (2015B) USING 355 KHZ IN OXYGEN ATMOSPHERE AND (RIGHT) YASUI ET AL. (2007) USING 300 KHZ IN AIR ATMOSPHERE..... | 34 |
| FIGURE 20: MATLAB CODE FOR THE IMPULSE FUNCTION | 35 |
| FIGURE 21: THE USE OF THE NUMERICAL SIMULATIONS OF MEROUANI ET AL. (2015B) TO DETERMINE THE FRACTION OF EACH SPECIES IN THE BUBBLE..... | 36 |
| FIGURE 22: THE USED NUMERICAL SIMULATIONS OF YASUI ET AL. (2007) TO DETERMINE THE FRACTIONS OF THE GENERATED SPECIES IN AN AIR BUBBLE..... | 38 |
| FIGURE 23: CIPROFLOXACIN REACTION AND REACTION RATE CONSTANT WITH HYDROXYL RADICAL | 39 |
| FIGURE 24: ACETAMINOPHEN REACTION AND REACTION RATE CONSTANT WITH HYDROXYL RADICAL | 40 |
| FIGURE 25: SIMULATION RESULTS IN AN OXYGEN ATMOSPHERE USING 1 HOUR (3600 s) OF SONICATION. CONCENTRATIONS ARE IN MOLES PER LITRE (M) AND TIME IN SECONDS. THE USED VALUE OF POWER WAS 1.06E-7. THE NAMES OF THE COMMON REACTIVE SPECIES: OR IS OXYGEN RADICAL, HR IS HYDROGEN RADICAL, HOR IS HYDROXYL RADICAL, H2O2 IS HYDROGEN PEROXIDE, HO2R IS PERHYDROXYL RADICAL AND O3 IS OZONE. PLOT CREATED WITH MATLAB | 41 |
| FIGURE 26: SIMULATION RESULTS IN AN OXYGEN ATMOSPHERE USING IMPULSE SONICATION OF 30 SECONDS ON-10 SECONDS OFF. CONCENTRATIONS ARE IN MOLES PER LITRE (M) AND TIME IN SECONDS. THE USED VALUE OF POWER WAS 1.06E-7. THE NAMES OF THE COMMON REACTIVE SPECIES: OR IS OXYGEN RADICAL, HR IS HYDROGEN RADICAL, HOR IS HYDROXYL RADICAL, H2O2 IS HYDROGEN PEROXIDE, HO2R IS PERHYDROXYL RADICAL AND O3 IS OZONE. PLOT CREATED WITH MATLAB | 42 |
| FIGURE 27: CALIBRATION RESULTS FOR SHORT SONICATION TIMES (20 MINUTES). THE DOTS ARE EXPERIMENTALLY FOUND, THE LINES REPRESENT THE SIMULATION DATA | 43 |
| FIGURE 28: CALIBRATION RESULTS OF LONG SONICATION TIME (2.5 HOURS). THE BLUE DOTS ARE THE EXPERIMENTALLY FOUND CONCENTRATIONS, THE LINES ARE THE PROFILES FOUND BY SIMULATIONS..... | 44 |
| FIGURE 29: CALIBRATION RESULTS OF LONG PERIOD (2.5 H) CHANGING THE OH/H ₂ O ₂ FRACTION RATIO. THE VALUES IN THE LEGEND ARE THE FRACTIONS USED IN THE SIMULATIONS AND THE POWER VALUE IS PRESENTED AFTER THE "-". DOTS ARE THE EXPERIMENTALLY FOUND VALUES, THE LINES ARE SIMULATION. | 45 |
| FIGURE 30: COMPARATION OF THE PH FOR LONG TERM EXPERIMENTS. THE DOTS INDICATE THE EXPERIMENTAL DATA, THE LINE IS THE PROFILE FOUND FROM SIMULATION | 46 |
| FIGURE 31: COMBINED RESULTS OF THE DEGRADATION OF 3.31 μM PHARMACEUTICAL COMPOUNDS. THE DOTS ARE PRESENTING THE EXPERIMENTAL DATA, THE LINES THE SIMULATION DATA. THE SIMULATIONS WERE DONE USING POWER = 1.06E-7 | 47 |
| FIGURE 32: DEGRADATION OF 40 μM CIP, EXPERIMENTAL RESULTS COMPARED WITH SIMULATIONS. THE BLUE DOTS INDICATE THE EXPERIMENTAL RESULTS AND THE LINE THE SIMULATION RESULTS. REACTION RATE CONSTANTS WERE SET AS K _{1,CIP} = 2.15E+8 AND K _{2,BY-PRODUCT} = 2.15E+10 | 48 |

FIGURE 33: COMPARATION OF THE H_2O_2 CONCENTRATION DURING SONICATION IN PRESENCE AND ABSENCE OF CIP. DOTS ARE PRESENTING THE EXPERIMENTAL DATA AND THE LINES THE SIMULATIONS..... 48

List of tables

| | |
|-----------------------------------------------------------------------------------------------------------------|----|
| TABLE 1: OXIDATIVE POWER COMMON OXIDIZING SPECIES (AUDENAERT, 2012) | 2 |
| TABLE 2: BUBBLE RADIUS RANGE AND OPTIMAL BUBBLE RADIUS FOR DIFFERENT FREQUENCIES (MEROUANI ET AL., 2013B) | 7 |
| TABLE 3: INLINE TYPES..... | 24 |
| TABLE 4: LIST OF THE GENERATED MATLAB FILES | 27 |
| TABLE 5: CHROMATOGRAPHIC DETAILS FOR ACE AND CIP | 30 |
| TABLE 6: FRACTIONS OF THE SPECIES OBTAINED FROM NUMERICAL SIMULATIONS OF MEROUANI ET AL. (2015B)..... | 36 |
| TABLE 7: REACTIONS USED IN THE CHEMICAL MODEL FOR US RADIATION IN OXYGEN SATURATED WATER | 37 |
| TABLE 8: FRACTIONS OF THE SPECIES OBTAINED FROM NUMERICAL SIMULATIONS OF YASUI ET AL. (2007) | 38 |
| TABLE 9: REACTIONS USED IN THE CHEMICAL MODEL FOR US RADIATION OF AIR SATURATED WATER | 39 |
| TABLE 10: COMPARATION OF PRODUCTION FRACTIONS OF BOTH MODELS (OXYGEN AND AIR ATMOSPHERE) | 45 |

CHAPTER 1: INTRODUCTION

1.1 General

Because the growing use of pharmaceuticals and personal care products (PPCP) all over the world, more and more of these components end up in wastewater, tap-water and receiving streams. The concentrations are at this moment very low (parts per trillion to parts per billion). The low concentrations are (still) not dangerous for human beings but, it is for the environment. Still, these PPCP's have high metabolic activity and in this turn, it can create antibiotic resistance bacteria, mutations and/or mortality of animal species on land or in water. Especially, PPCP's can be accumulated in aquatic life e.g., in fish. A.J. Ebele et al. (2017) discussed this in their paper as a treat for human life in the near future. (Liu and Wong, 2013; Ren et al., 2021; Sammut Bartolo et al., 2020) Lui and Wong evaluated several municipal wastewaters in China in 2013 looking for contamination with PPCP's. They found that in some places even tracks of PPCP's were found in tap water. Concentrations were found in terms of $\mu\text{g}\cdot\text{L}^{-1}$ in wastewater and in sludge in terms of $\mu\text{g}\cdot\text{g}^{-1}$. They also mentioned that in the future this could cause potential environmental and health risks in the near future.

Because of the importance to reduce the concentration of those components in our environmental system, advanced oxidation processes (AOP) are extremely helpful in oxidising those components that can't be decomposed by activated sludge systems due to long retention times and selectivity of the micro-organisms in the activated sludge system. Implementing an AOP method in a purification processes can help to solve these specific problem of low bio-degradability (Gwadi, 2011). Also, because of the activated sludge treatment of the municipal wastewaters, unpredictable transformation products can occur due to the interaction with the biomass. Those transformation products can have an even more toxic effect on the environment (Ren et al., 2021).

AOP refers to a set of chemical treatment procedures designed to remove organic pollutants in water and wastewater by oxidation reactions with hydroxyl radicals ($\cdot\text{OH}$). There are several paths to create the hydroxyl radicals (Navarro, 2021). Most of the AOP techniques currently used, are showed in Figure 1.

STUDY OF RADICAL CHEMISTRY IN ADVANCED OXIDATION PROCESSES BASED ON ULTRASOUND RADIATION IN WATER FOR PHARMACEUTICAL DRUGS REMOVAL

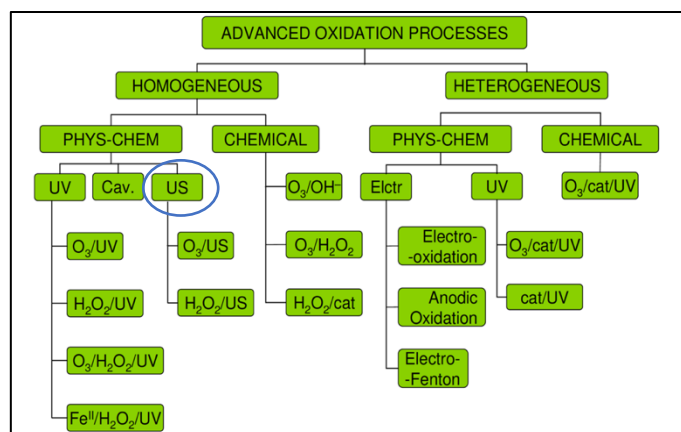


Figure 1: AOP techniques, adapted from J. Navarro

The hydroxyl radicals can be obtained in many ways using chemical or physical methods. Depending on the fact if the process has one or more phases, the process is heterogeneous (solid-liquid phase) or homogenous (only liquid phase).

The hydroxyl radical is the second-best oxidant regarding to the oxidation potentials (Table 1). This means that beside fluorine, it can oxidise everything in a matrix. The reaction rate constants for hydroxyl oxidations in aqueous phase variate around 10^6 - $10^{10} \text{ M}^{-1} \text{ s}^{-1}$ (Kanakaraju et al., 2018). Also, derivative products from the hydroxyl radicals as ozone and hydrogen peroxide are also high listed.

Table 1: Oxidative power common oxidizing species (Audenaert, 2012)

| Oxidizing species | Oxidation potential (V vs SHE) |
|----------------------------------------------|--------------------------------|
| Fluorine (F) | 3.03 |
| Hydroxyl radical ($\cdot\text{OH}$) | 2.80 |
| Atomic oxygen (O) | 2.42 |
| Ozone (O_3) | 2.07 |
| Hydrogen peroxide (H_2O_2) | 1.78 |
| Hydroperoxyl radical ($\text{HO}_2\cdot$) | 1.70 |
| Permanganate (MnO_4^-) | 1.68 |
| Hypobromous acid (HOBr) | 1.59 |
| Chlorine dioxide (ClO_2) | 1.57 |
| Hypochlorous acid (HOCl) | 1.49 |
| Chlorine (Cl_2) | 1.39 |

The AOP technique that has been investigated in this thesis project is the application of ultrasound (thereafter US, encircled in blue in Figure 1).

US for water treatment is well known in the literature for several decades but there are some problems when scaling-up the reactors to industrial scale. No installation have been reported in the literature with only using US. Thus, US is used in hybrid techniques like UV/US, O_3 /US, US/ H_2O_2 or a mix of them. The efficiency of the energy conversion is too low using only US, so the costs increase. Mahamuni and Adewuyi (2010) calculated an estimated cost for several AOP techniques and one of the results is shown in Figure 2.

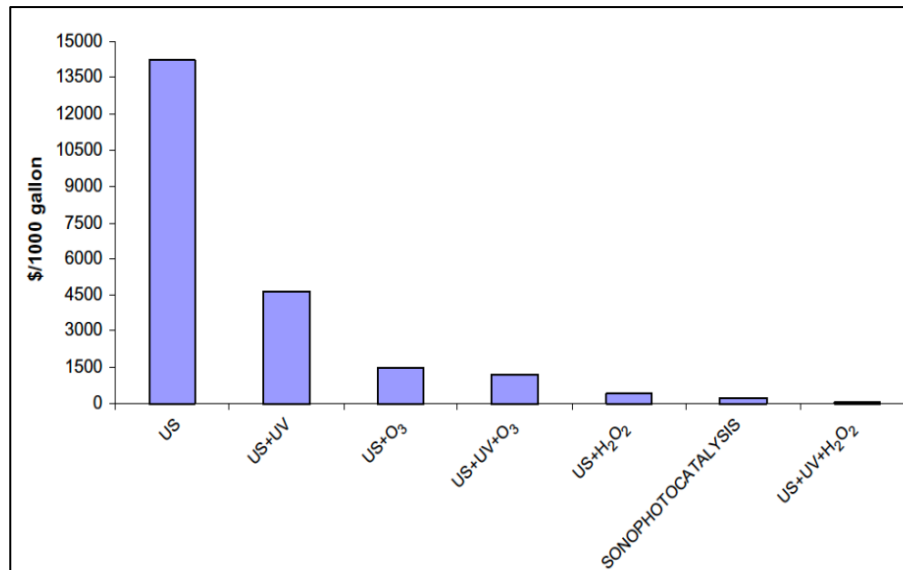


Figure 2: Costs of AOP involving US for dye removal, Mahamuni and Adewuyi (2010)

The results show a big cost difference between US or the hybrid techniques. The biggest economical issue for only working with ultrasound is the high energy densities that are needed. The high energy densities are due to the efficiency of the transducers that are rather low (Mahamuni and Adewuyi, 2010). But, when looking forward in time, there is expected that the efficiency of the apparatus will increase due to innovation. This will cause a major decrease in operational cost so the US will be more attractive to implement in the industry. (Ingole and Khedkar, 2012)

In this thesis study the focus lies on chemical modelling of the US radiation in water. Additionally, there will be tried to extend the model for pharmaceutical removal.

1.2 Overview

The following items will be discussed in the next chapters: in chapter two, a literature review of the used techniques and the equations that describe the dynamics to build the model will be reviewed in detail. For a better understanding of the objectives of this work, they are presented at the end of the literature review. Section three will give some more information of the used materials and methods. In here a concrete description of the used simulation programs and laboratory tests will be given. The fourth section will describe the dynamic model that is obtained from the literature and laboratory tests. In chapter five the results of the simulations will be showed and discussed. At last, a general conclusion of the master thesis will be given in section six.

The thesis also includes a short budget cover about the work which is placed behind the references at the end of this scripton.

CHAPTER 2: LITERATURE REVIEW

2.1 Introduction

The type of chemistry that describes the kind of chemical reactions that occur when exposing US to the solution is called *Sonochemistry*. Sonochemistry is not only for purification purposes but has a much wider field of use. It is also used for (bio)chemical engineering (e.g., nanomaterials, crystallisation and metallic alloys) and medicinal uses. Another term used for the forming of radical species out of water using US is *sonolysis*. (Gogate and Patil, 2016; Son, 2016a).

The difficulty to obtain a dynamic kinetic model is to couple the chemical kinetics to the physical phenomena that are taking place. These phenomena are the bubble dynamics and the characteristics of the bubbles (lifetime, radius, concentration, ...). Both are not easy to determine and depend on many factors. (Bhangu and Ashokkumar, 2016; Mahamuni and Adewuyi, 2010; Merouani et al., 2015b, 2014; Yasui, 2016)

Various papers show that US can be used for removal of pharmaceuticals and other (organic) pollutants. (Camargo-Perea et al., 2021; Torres-Palma and Serna-Galvis, 2018)

In the next sections the sonochemical phenomena are described together with the mathematical approaches that can be used and the configurations possible for US treatment.

2.2 Acoustic cavitation

2.2.1 General

Cavitation is a phenomenon that is discovered by Thornycroft in 1895, when doing research on damaged torpedo boats. He found that, when negative pressures (< 1 atm) appear due to high speeds (in the case of the torpedo boats), small bubbles are formed. When these bubbles implode, high damage was done to propellers of the boat.

The same happens when applying a high frequency pressure wave (ultrasound) through a liquid. The irradiation of a sinusoidal pressure wave at high frequency (>25 kHz) causes pressure changes inside the water. At the places of rarefaction, small (invisible with the naked eye) bubbles are formed. They grow in an oscillating nonlinear way until a point where the bubble collapses (Figure 3). This phenomenon is called acoustic cavitation. (Chatel et al., 2016; Merouani et al., 2015b, 2014; Son, 2016a; Yasui, 2018)

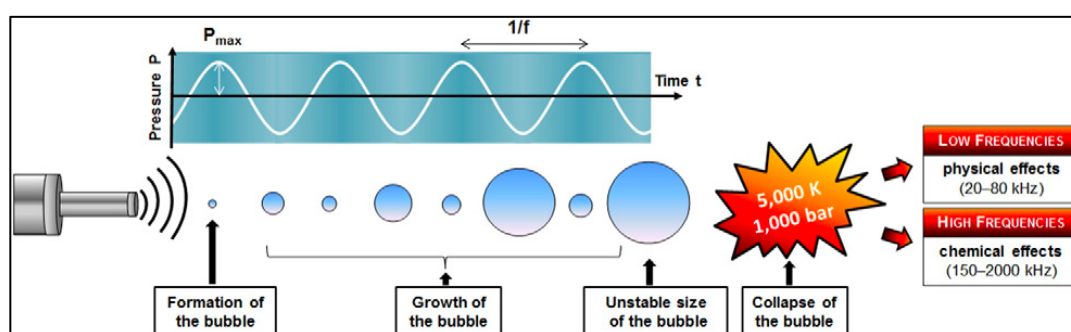


Figure 3: Formation and collapse of an acoustic bubble, Chatel et al. (2015)

In acoustic cavitation bubbles, high temperatures (± 5000 K) and pressures (± 1000 atm) occur for a very short time. Due to the extreme temperature and pressure, water and dissolved gasses (e.g., air) that are trapped inside the bubble, decompose forming very reactive species as H^\bullet , $^\bullet OH$, $^\bullet O_2H$, $^\bullet O$ and $^\bullet N$. The obtained radicals can react forming ozone (O_3), hydrogen peroxide (H_2O_2) and some other compounds. The main objective is to get a high concentration of the most reactive species, which in this case is the hydroxyl radical ($^\bullet OH$). Depending on the ultrasound frequency that is used, the effects are mechanical for low frequencies (< 100 kHz) and chemical for high frequencies ($0.1 - 2$ MHz). The formation, growth and implosion phase happen in terms of microseconds (10^{-6} s). In Figure 4, an acoustic radiation is shown together with the variation of the bubble radius. There is seen that the bubble collapses within some microseconds. The bubble dynamics will be further described in next section. (Braeutigam, 2016; Chatel et al., 2016; Ge, 2015; Merouani et al., 2015b, 2014; Yasui, 2018)

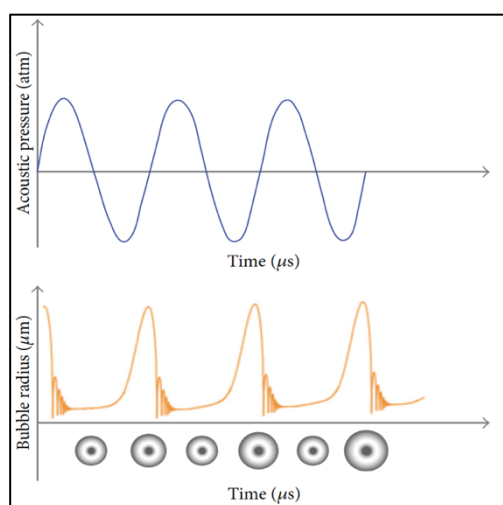


Figure 4: The bubble radius oscillation due to an acoustic pressure wave, Ge (2015)

2.2.2 Bubble dynamics

2.2.2.1 Bubble radius

The mathematical approaches for these kinds of dynamics are described as non-linear differential equations. These complex differential equations must be solved using numerical methods. There are several equations that can be used to describe the dynamics, more specific the radii, of a cavitation bubble.

The first approach was described by Lord Rayleigh in 1917. The model has been improved by many others and is now been used as the Rayleigh–Plesset–Noltingk–Neppiras–Poritsky equation 2.1. (Moholkar, 2016)

$$R\ddot{R} + \frac{3}{2}\dot{R}^2 = \frac{1}{\rho} \left[P_0 + \frac{2\sigma}{R_0} - P_v \left(\frac{R_0}{R} \right)^{3\gamma} + P_v - \frac{2\sigma}{R_0} - \frac{4\mu}{R} \dot{R} - (P_0 + P(t)) \right] \quad (2.1)$$

The dots indicate time derivatives, R is bubble radius, ρ is the liquid density, σ is the surface tension, μ is the liquid viscosity, P_0 is the pressure inside the bubble, P_v is the pressure vapor of water, γ is the ratio of specific heat capacities of the vapor/gas mixture (c_p/c_v) and $P(t)$ is equal to: $P(t) = P_A \sin(2\pi ft)$ with P_A is the acoustic amplitudes, t is the time and f is the frequency. P_A is correlated to the intensity of the sound wave. It can be described as:

$$P_A = \sqrt{2I_a \rho_L c} \quad (2.2)$$

with I_a , the intensity of the acoustic power unit. The equation and its derivatives equations are no longer valid once the bubble collapse is violent. A violent collapse appears when the collapse speed is close to the Mach number. The Mach number (M) is equal to the fluid velocity (\dot{R}) divided by the sound velocity (c).

In the more recent literature, the Keller-Mikis equation (2.3) is used instead which includes the effects near Mach number (Merouani et al., 2015b, 2014; Yasui, 2018).

$$\left(1 - \frac{\dot{R}}{c} \right) R\ddot{R} + \frac{3}{2} \left(1 - \frac{\dot{R}}{3c} \right) \dot{R}^2 = \frac{1}{\rho_L} \left(1 + \frac{\dot{R}}{c} \frac{R}{c} \cdot \frac{d}{dt} \right) \cdot \left[p - p_\infty - \frac{2\sigma}{R} - 4\mu \frac{\dot{R}}{R} + P_A \sin(2\pi ft) \right] \quad (2.3)$$

With c is the speed of sound in the liquid, p is the pressure inside the bubble and p_∞ is the ambient static pressure. For equation (2.3), there are derivate equations that describe similar dynamics (Moholkar, 2016; Yasui, 2018, 2001).

The formulas showed before can be used in different dynamic models to calculate the bubble radius in experimental conditions. The outcome of the radii is well described by different researchers and lot of simulation is done in the past. Due to bubble distribution and bubble interaction, the radius of each bubble can variate within a range. Because of distribution in bubble radius, calculations in the literature were done using the mean of the bubble radius range. In a study of Merouani et al. (2013b) the following values (Table 2) were determined using an acoustic amplitude of 1.5 and 2.5 atm:

Table 2: Bubble radius range and optimal bubble radius for different frequencies (Merouani et al., 2013b)

| Frequency (kHz) | Theoretical range of bubble radius (μm) | | Optimal bubble radius (μm) | |
|-----------------|------------------------------------------------------|-----------|-----------------------------------------|---------|
| | 1.5 atm | 2.5 atm | 1.5 atm | 2.5 atm |
| 200 | 1.2-13.5 | 0.33-18.5 | 5.0 | 8.0 |
| 300 | 1.5-8.5 | 0.35-12.5 | 3.5 | 5.2 |
| 500 | 2.0-5.0 | 0.38-7.0 | 2.7 | 3.0 |
| 1000 | 1.25-3.2 | 0.45-3.2 | 1.85 | 1.5 |

The table shows that when applying higher frequencies, the bubble radius and the range become smaller. When applying more acoustic amplitude, the range of radius is also wider. In the tests it was also clear when using 200 and 300 kHz, the optimal radius increased linearly with the acoustic amplitude.

The biggest problem with these very complex second order differential equations is that changing one variable can give very different solutions. This means that when using these equations, the variables have to be as precise as possible (Varga and Paál, 2015).

2.2.2.2 Bubble temperature and pressure

The temperature and pressure inside the bubble can be described as follows:

$$T = T_{\infty} \left(\frac{R_{max}}{R} \right)^{3(\gamma-1)} \quad (2.4)$$

$$p = \left[p_v + p_{g0} \left(\frac{R_0}{R_{max}} \right)^3 \right] \left(\frac{R_{max}}{R} \right)^{3\gamma} \quad (2.5)$$

With T_{∞} is the bulk temperature, R_{max} is the maximum radius of the bubble, R_0 is the ambient bubble radius, p_v is the vapor pressure of water, p_{g0} is the gas pressure in the bubble at $R=R_0$ and equals $p_{g0} = p_{\infty} + (2\sigma/R_0) - P_v$ and γ is the polytropic index of the gas inside the bubble (equals C_p/C_v). These formulas can only be used when there's assumed that the bubble expansion is isothermal, that the implosion phase is treated as adiabatic, temperature and pressures are equal at every place in the bubble and that the bubble wall velocity is slower than speed of sound in the liquid (Notice that this latter assumption is not equal to the conditions of the Keller-Mikis equation). This means heat and mass transfer are not taking in account. Also, these formulas only are fully correct when no reactions occur but in most cases, these formulas give realistic simulation results (Gielen et al., 2016; Merouani et al., 2015b).

Regarding to a work about the estimation of bubble temperatures using methyl radical recombination (MRR) of Ciawi and co-workers (Ciawi et al., 2006), the temperature inside the bubble is strongly correlated to the applied frequency. The temperatures that were found were 3400 ± 200 , 3700 ± 200 and 4300 ± 200 K for 20, 1056 and 355 kHz respectively. In the same study, they mentioned that the maximum temperatures for acoustic cavitation bubbles will be found in pure water. They did not report a value for the minimum or maximum temperature. Regarding to the study of Merouani et al. (2014), in a multi-bubble environment the temperature range for sonochemistry is between 750 and 6000 K. The temperature is very depending on the dissolved gasses that are present. The influence of dissolved gasses will be given in section 2.3.2.

The pressures that occur in the bubbles are estimated starting from 500 bar until 4000 bar. Merouani et al. (2014) reported an optimal pressure of 2500 bar for the yield of hydroxyl radicals. These values should be considered with reservation due to the lack of information about the range of pressures that occur in simulations. (Ashokkumar, 2011; Merouani et al., 2014)

2.2.2.3 Number of bubbles

Because of the production of the hydroxyl radicals takes place inside of the cavitation bubbles, it is important to have an estimation of the number of bubbles that are inside de reactor. Naidu et al. (1994) mentioned in their research about modelling of a batch sonochemical reactor that the number of bubbles that collapse per time-unit and reactor volume only depend on the operating parameters i.e., frequency, power input and the reactor configuration.

More recently, Merouani et al. (2015a) proposed a semi empirical formula to determine the number of active bubbles by using equation 2.6.

$$N = \frac{r_{H_2O_2}}{n_{H_2O_2} 0.5(n_{OH\cdot} + n_{HO\cdot_2})} \quad (2.6)$$

The reaction rate of hydrogen peroxide can be found experimentally using e.g., iodometric measurement. The number of moles (n_x) of hydrogen peroxide, hydroxyl and perhydroxyl radical can be obtained using a bubble dynamic model (Merouani used equation 2.3) to predict the number of species trapped inside the bubble.

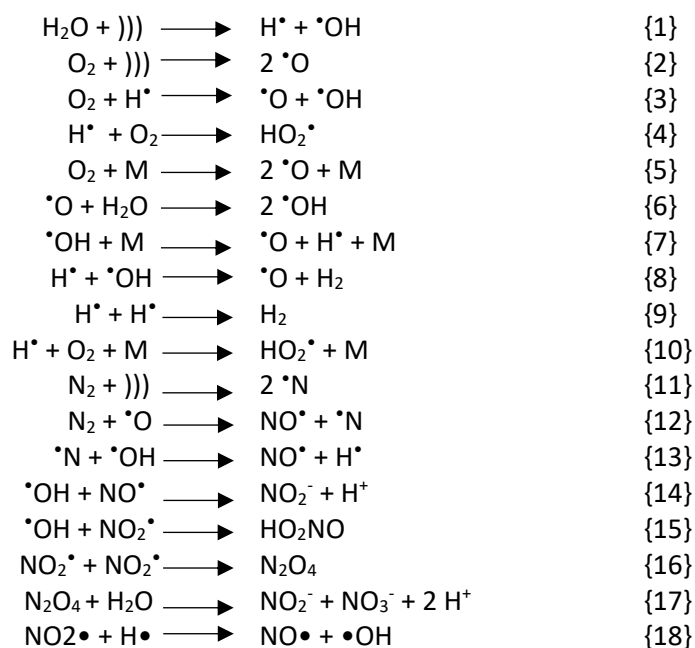
2.2.3 Chemical kinetics

In an acoustic cavitation bubble, due to the high temperatures, every component will be either pyrolyzed, for organic (volatile) matter, or will decompose in the radicals (see further). The radicals that are formed will interact with each other inside the cavitation bubble or most likely react with organic matter near the bubble after collapse. The kinetics for this kind of phenomena are difficult to describe due to lot of influence parameters. (Bhangu and Ashokkumar, 2016; Merouani et al., 2014; Yasui, 2018). In following section, a deeper description of the chemical kinetics inside the bubble will be given together with the influence parameters.

2.2.3.1 Reactions inside or near the bubble

In general, due to the high temperatures and pressure in the bubbles, gaseous water and air/oxygen trapped in the bubble decompose thermally into radicals. The reactions are described in many papers (Bhangu and Ashokkumar, 2016; Kanakaraju et al., 2018; Merouani et al., 2015a; Torres-Palma and Serna-Galvis, 2018; Yasui et al., 2007).

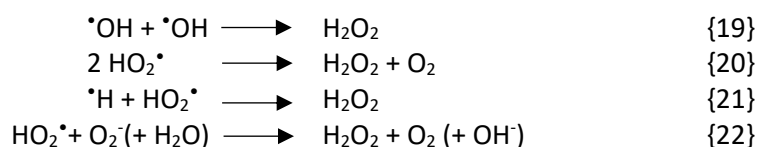
Some of the most common reactions that are taking place (inside the bubble) in oxygen saturated water (reactions 1-10) and in air (O₂/N₂) saturated water (reactions 1-18) are shown below:



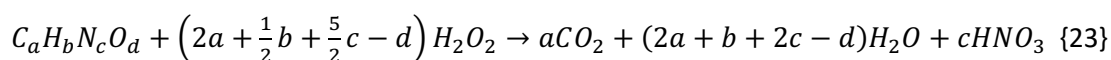
Note that these reactions are reactions occurring inside the collapsing bubbles. The reactions occurring in aqueous solution will be deeply described in chapter 3. The US radiation in the reactions are indicated with “)”). The radicals formed in reactions 1, 2 and 11 can interact with each other or with organic matter (after the bubble collapse).

When working under air atmosphere, the nitrogen radicals will interact with oxygen and water, forming nitric acid as end product (reactions 14 and 17 produce acidic protons). (Mack and Bolton, 1999; Yasui et al., 2007). This indicates that during experiments, pH will decrease with time. To prevent this to happen, air can be replaced by oxygen or noble gasses (hydroxyl yield improvement: He<Ne<Kr<Ar<Xe) (Brotchie et al., 2010; Torres-Palma and Serna-Galvis, 2018). The M in the reactions, called a third body, is most of the time a noble gas. Due to high temperatures and pressures inside the cavity, high energy levels are present. So, because of interference of a molecule with M, energy can be transferred from M to the molecule which turn then has enough energy to break the molecules into radical species (Brotchie et al., 2010).

As mentioned before, the most dominant reactive species in sonochemistry is the hydroxyl radical ($\cdot\text{OH}$). This radical, together with the hydroperoxyl radical ($\text{HO}_2\cdot$) can react forming hydrogen peroxide (H_2O_2) as showed in the following reactions (Buxton et al., 1988; Torres-Palma and Serna-Galvis, 2018):



Hydrogen peroxide is more stable and can interact (not selective) with for example, pharmaceuticals or other pollutants near the bubble collapse location. Li et al. (2021) used the following empirical reaction {23} to describe the degradation of pharmaceuticals with hydrogen peroxide as reactant:



When working in a multi component matrix (as in wastewater or experiments with more than one target molecule) it is possible that some target molecules will be way more degrade than others due to their hydrophilic/hydrophobic properties. When bubbles are formed, a more hydrophobic zone is created around the bubble. This causes hydrophobic pollutants to move closer to the bubbles and also making them more likely to react with hydroxyl radicals or other reactive species that appear at the bubble wall or when the bubble collapses. Eventually, hydrophilic molecules will move further away from the bubbles causing them less likely to react with the sonolytic species (Camargo-Perea et al., 2021). Ince et al. (2001) even mention that when low frequencies are applied, only hydrophobic components are able to react. They also declare that hydrophobic components are able to merge through the bubble wall inside the bubble. When these components enter the bubble, they get pyrolyzed immediately. When applying higher frequencies (300-1000 kHz) this latter phenomena of migration through the bubble wall is rather small due to very small lifetimes of the bubble (0.4 μs compared to 20 μs when using 20 kHz).

2.2.3.2 Chemical kinetics

To have a detailed trace of the concentration for a time t , a kinetic model is needed. This kinetic model is a set of ordinary differential equations (ODE's) of the chemical kinetics supplemented with an additional term Φ (ϕ) that describes the generation of species c_i due to, in this case, the radiation of US. A general representation of the mathematical equation is:

$$\frac{dc_i}{dt} = \phi + \sum_j R_{ij} \quad i = 1, \dots, n, \quad j = 1, \dots, r. \quad (2.7)$$

With c_i the concentration value of the i th species, R_{ij} a vector that describes all the reaction rates of all reactions r involving all species i , n and r are the number of species and number of reactions in the scheme, respectively. The reaction rate vector R_{ij} is a result of all the individual reaction rates multiplied by a stoichiometric matrix, $Z^{(ix)}$ (Navarro, 2021).

$$R_{ij} = v_i^T \cdot r_j \quad (2.8)$$

A stoichiometric matrix $Z^{(ix)}$ is a matrix with i columns and j rows that contains the stoichiometric value of all the species i for all the j reactions. This means that the matrix has as many columns and rows as there are species and reactions respectively.

The reaction rate r_i is in turn a function of the reaction rate constant k (which is temperature depending, according to the Arrhenius equation 2.10) and the concentration of the involving species.

$$r_j(T, c) = k_j(T) \prod_i c_i \quad (2.9)$$

$$k_j(T) = A \cdot e^{-\frac{E_a}{RT}} \quad (2.10)$$

With A as the pre-exponential constant, E_a the activation energy, R as the gas constant and T the temperature.

This model is used by Ershov and Gordeev (2008) to describe radiolysis of water. They used as source-term: $\phi = G_i \cdot I$ with G_i as the chemical yield for species i (in molecule/eV) and I the ionising dose rate (in eV).

For US irradiation Merouani et al. (2015) suggested a source-term related to the number of bubbles that are produced. Equation 2.7 can be written as follows:

$$\frac{dc_i}{dt} = N \cdot n_i + \sum_j R_{ij}(T, c) = f(T, c) \quad i = 1, \dots, n, \quad j = 1, \dots, r. \quad (2.11)$$

With N the number of bubbles and n_i number of moles of species i produces in a single bubble. N can be calculated using equation 2.6 described in section 2.2.2.3 Number of bubbles.

$$N = \frac{r_{H_2O_2}}{n_{H_2O_2}^{0.5} (n_{OH\cdot} + n_{HO_2\cdot})} \quad (2.6)$$

To use equation 2.6 you have to rely on experimental data and bubble dynamics simulations for the bubble radii. This means that the use of these equations needs a lot of effort and depend on all the reaction parameters as described in section 2.2.2.3.

Using a mathematical model as equation 2.11 results in a set of ODE's that can be classified as "very stiff" differential equations. To trace the concentration in time, using the initial concentrations of the species involved, numerical integration methods are used. For these integration methods, evaluation of the Jacobian of the derivative function is necessary (Damian et al., 2002):

$$J = \frac{\partial f(T, c)}{\partial c} \begin{bmatrix} \frac{\partial f_1}{\partial c_1} & \frac{\partial f_1}{\partial c_2} & \dots & \frac{\partial f_1}{\partial c_n} \\ \frac{\partial f_2}{\partial c_1} & \frac{\partial f_2}{\partial c_2} & \dots & \frac{\partial f_2}{\partial c_n} \\ \vdots & \vdots & \ddots & \vdots \\ \frac{\partial f_n}{\partial c_1} & \frac{\partial f_n}{\partial c_2} & \dots & \frac{\partial f_n}{\partial c_n} \end{bmatrix} \quad (2.12)$$

To describe the chemical kinetics in detail, simulation programs can be used. The one used in this work is KPP and will be discussed in Chapter 3.

2.3 Operational parameters

2.3.1 Soundwave properties

The overall efficiency of a sonochemical process depends of the numbers of bubbles formed and their size, which in turn depend on the characteristics of the sound wave itself (Merouani et al., 2015a). A soundwave is a pressure wave that can be described as a sinusoidal wave with an amplitude P_A and a frequency f . The pressure amplitude can be changed by changing the intensity of the power unit, as described in equation (2.3). In literature, the value of the acoustic amplitude variates between 1.5 and 10 atm (Merouani et al., 2013; Yasui et al., 2007, 2004).

$$\left(1 - \frac{\dot{R}}{c}\right) R \ddot{R} + \frac{3}{2} \left(1 - \frac{\dot{R}}{3c}\right) R^2 = \frac{1}{\rho_L} \left(1 + \frac{\dot{R} R}{c} \cdot \frac{d}{dt}\right) \cdot \left[p - p_\infty - \frac{2\sigma}{R} - 4\mu \frac{\dot{R}}{R} + P_A \sin(2\pi f t)\right] \quad (2.3)$$

The amount of acoustic power can be given just in watt's (W), power density ($W \cdot L^{-1}$) or as the power intensity I_a ($W \cdot cm^{-2}$). The power density seems to be the most common used way to indicate the acoustic power but regarding literature it depends on the researcher's preference. In a review study of Torres-Palma and Serna-Galvis (2018), they reported that when more power was applied a higher concentration and faster increase of hydrogen peroxide was detected.

Most of the time, the frequency used in US for chemical effects starts around 100 kHz. Most number of radicals are found when using frequencies between 200-500 kHz. Frequency can be increased to higher values (500 kHz or more) but for the degradation of pharmaceuticals, frequencies around 300 kHz are often used (Camargo-Perea et al., 2021; Torres-Palma and Serna-Galvis, 2018). Mousally et al. (2019) detected higher degradation yields for dibenzothiophene when using 352 kHz instead of 20 kHz.

2.3.2 Dissolved gasses

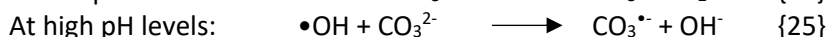
Inside the bubbles, pressure and temperatures change depending on the dissolved gasses that are present in the solution. When higher temperatures and pressures occur inside the bubble, more radicals can be formed. The optimal temperature (giving the highest hydroxyl yield) was set by Merouani et al. (2014) at 5200 ± 200 K when using oxygen saturated atmosphere. Yasui et al. (2004) discussed that, when using oxygen bubbles, temperatures can go higher without effecting the hydroxyl production (6000 K or even higher). When using air atmosphere, the maximum temperature has to be 5500 K because the radicals will oxidate the nitrogen.

Regarding a review study of Torres-Palma and Serna-Galvis (2018), CO_2 hinders the degradation of organic pollutants. They suggest using an Ar/O_2 mixture for best results. The presence of organic matter, especially volatile species, also reduces the temperature inside the bubble, due to the consumed enthalpy to evaporate the components (Yasui, 2018).

Generally, Son (2016) described that argon gets the highest temperatures inside the bubbles and becomes more effective for pyrolysis applications. Oxygen gas and air seemed to have better results regarding indirect radical reactions.

2.3.3 Dissolved ions

Dissolved ion components also play a big role in the sonolytical efficiency. In most water sources, inorganic ions and traces of metal ions are present. They can cause enhancement or weakening of the sonolytical reactions. Aqueous anions as nitrate (NO_3^-), sulfate (SO_4^{2-}), chloride (Cl^-), bicarbonate (HCO_3^{2-}) and bromide (Br^-) can act as scavengers for the reactive hydroxyl radical. This was investigated by Gao et al, (2013) when looking into the affecting parameters of sonolytic degradation of sulfamethazine. They found that, when the anions were present in the solution, the sonolytic effect weakened in following order of inhibition degree: $\text{NO}_3^- > \text{Cl}^- > \text{SO}_4^{2-}$. On the contrary, Br^- and HCO_3^{2-} improved the degradation. Some other papers show that bicarbonate has a rather bad effect on sonolytic reactions, thus it depends on the target molecule (Son, 2016b). In a recent research of Camargo-Perea et al. (2021) is showed that for removal of pharmaceuticals using US at 375 kHz, the presence of bicarbonate anion enhanced the degradation of components that were further away of the bubbles. This could be explained due to a less reactive bicarbonate radical that is formed. Depending on the pH of the solution, scavenger reactions for carbonate/bicarbonate are the following (Mehrvar et al., 2001):



Regarding to reactions in waters with high conductivities as seawater, Mousally et al. (2019) studied the influence of seawater to the degradation of benzothiophene and detected the same degradation rates then in deionized water.

Beside inorganic anions, metallic ions also influence the reaction dynamics. Dissolved iron ($\text{Fe}^{2+}/\text{Fe}^{3+}$) can act as a catalyst for the formation of hydroxyl radicals (see Figure 5). These reactions are so called Fenton reactions and this technique is also listed as an advanced oxidation processes (Barbusinki, 2009; Gao et al., 2013).

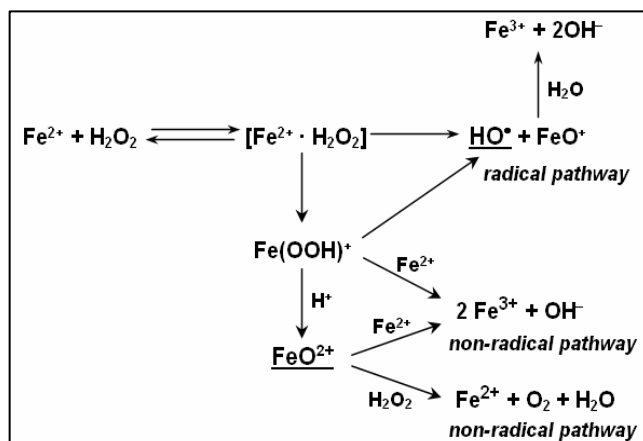


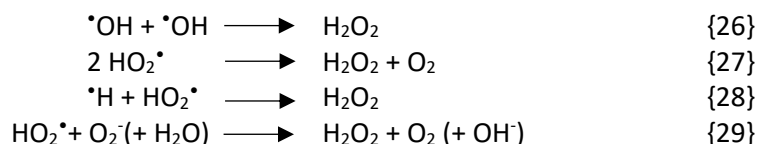
Figure 5: Fenton reaction pathway in absence of organic substances, from Barbusinki (2009)

2.3.4 Reaction time

The reaction time of the chemical reactions inside the bubble are very short. The reactions stop when the reactive species aren't available anymore in the solution. The way of stopping those species to occur is to stop irradiation of the US waves. The cavitation yields increase with time of operation until a certain point where the increase becomes marginal (Gogate and Patil, 2016). Regarding to several studies about different component degradation, (Camargo-Perea et al., 2021; Mousally et al., 2019; Okitsu et al., 2016; Torres-Palma and Serna-Galvis, 2018) the sonofication time was about 30 to 60 minutes. When applying too long, the cost will increase against the small amount of additional yield that is created. Also, the target molecules and matrix can affect the degradation rates.

2.3.5 H_2O_2 concentration

To follow up the amount of (hydroxyl) radicals produced it is possible to detect the amount of hydrogen peroxide (H_2O_2) that is formed due to the recombination of the radicals as in reactions 19-22.



The concentration of the hydrogen peroxide can be determined by using titration or spectrophotometric techniques as iodometry.

2.4 Reactor configurations

The soundwave can be produced in different kind of ways, depending on the frequency and intensity needed. In general, there are two types of sources. The most common one is an ultrasonic horn (I). In more recent studies, the transducers are directly installed on the vessel wall itself instead of using a horn (II). Sonochemical reactors can be designed with two parallel plates irradiating the same or different frequencies, tubular models with reactors irradiation form both sides or one irradiation side with a reflector-side or a flow cell-configuration with transducers attached to the vessel. It is important, when designing a reactor for a specific application that there should be a uniform distribution of irradiation throughout the vessel with as high cavitational yield as possible (Gogate and Patil, 2016).

When using an ultrasound reactor, cooling is necessary to keep temperatures constant. Temperatures increase due to the sonolytical effects. Most of the time this is done by using a cooling jacket and water as heat transport fluid (Gogate and Patil, 2016; Merouani et al., 2015a).

2.4.1 Working principle of an US transducer

An US transducer is an apparatus which can convert electrical energy into mechanical energy. Transducers can be made out of organic polymers or piezoelectric ceramic materials. The latter one is most used as US transducer. A definition of ceramic material is: "A ceramic material may be defined as any inorganic crystalline material, compounded of a metal and a non-metal"(Subedi, 2013).

A more detailed drawing of piezoelectric transducers is showed in Figure 6. The transducer is made out of a piezoelectric crystal that is squeezed between two parallel electrodes. The electrodes are connected to an electric amplifier (when used as detector) or an alternating current supply (when used as a transmitter) (mrcophth.com, n.d.).

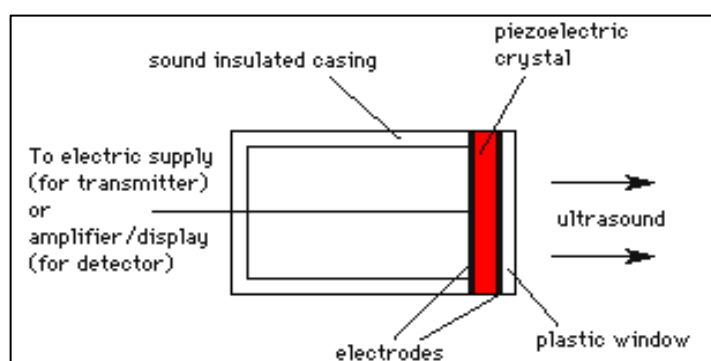


Figure 6: Piezoelectric transducer (source: <http://www.mrcophth.com/commonultrasoundcases/principlesofultrasound.html>)

The working principle of an ultrasonic transducer is based on the properties of that piezoelectric crystal. When applying an alternating current (AC) on the electrodes, a soundwave is generated due to atomic movements (indicated in Figure 7). In Figure 7, a piezoelectric ceramic crystal of lead-zirconatetitanate (PZT) is shown. Because of the alternating current, the titanium or zirconium kernel will move up and down generating mechanical vibrations and these vibrations create in turn a pressure wave.

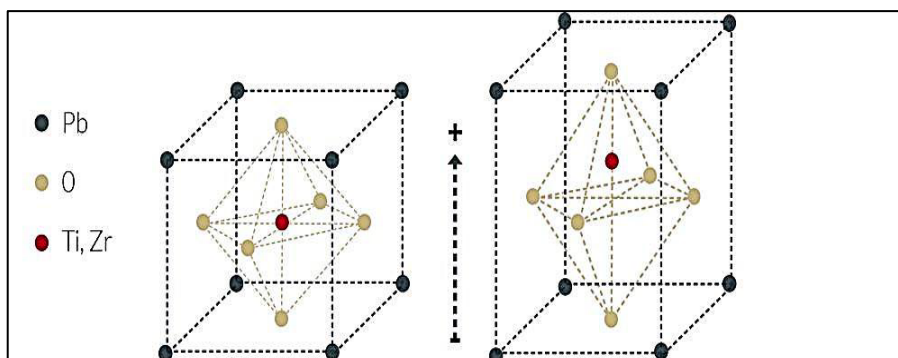


Figure 7: Structure and movement of a piezoelectric material, used from Haland (2017)

On the righthand side of Figure 7, an upgoing movement is indicated when applying a positive charge to the electrode above the crystal. By increasing the power and the frequency of the AC, a pressure wave with respectively higher amplitude and frequency is generated. Piezoelectric ceramics are most often used in sonochemistry due to their temperature resistance and their instability. Other common used ceramic crystals as BariumTitanate (BT) and leadniobate lithiumniobate (PBLN) are used for generating US waves. (Haland et al., 2017; piezodisk.com, 2018).

2.4.2 Sonochemical horn

A Sonochemical horn is simply a transducer where a horn is attached. The horn can be placed vertically or longitudinal, respectively (a) and (c) showed in Figure 8, inside the reaction liquid. Due to the horn shape, a lot of cavities are formed near the tip of the horn. Further away of the tip, less bubbles are formed. This means that the use of horns for bigger reactor volumes are an issue. Because of that, horns are often used in small laboratory tests. The configurations can in a batch or flow loop (Ge, 2015; Gogate and Patil, 2016). Regarding to the website of Dukane® (Dukane, 2010) horns are able to generate soundwaves till a maximum of 50 kHz. The problem with these horn types is that the frequency is fixed and only the intensity can be increased by applying more power to the unit.

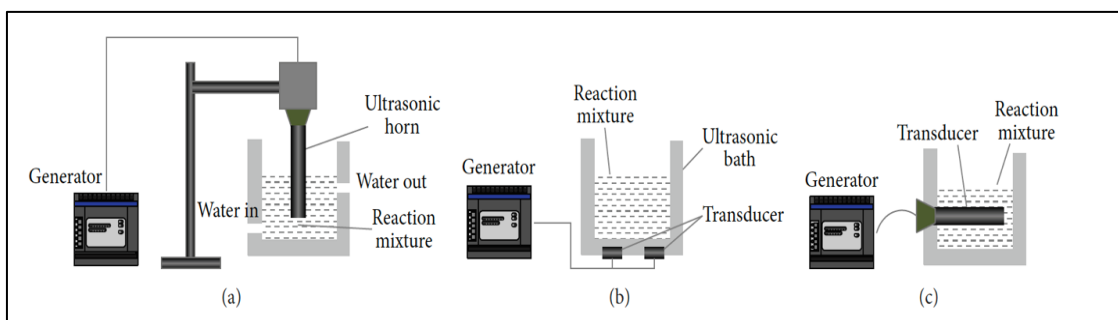


Figure 8: different ways of ultrasound reactors, used from C. Ge (2015)

2.4.3 Ultrasonic bath

A second way is to use ultrasonic transducers which are placed directly on the sides or underneath the reactor (see (b) Figure 8). It is possible to use the bath directly or place a reactor (for example, a smaller glass jar filled with the reactants) inside. These baths can generate US waves in a very wide range of frequencies regarding to the transducers used (50 kHz up to 200 MHz) (Tom Nelligan, n.d.). The general problem with the transducers is that they remain very small (about 4-6 cm diameter maximum, regarding to the companies Ultrason Group and Olympus IMS). Therefore, the capability to upscale these types of reactors are difficult. A solution to that is to generate a more tubular configuration with a transducer at the bottom of the cylinder. These ultrasonic baths can be used as batch reactor or as overflow reactor. (Gogate and Patil, 2016)

2.4.4 Multiple-frequency reactor

Gogate and Patil (2016) mentioned in their review study about sonochemical reactors that more recently some upscaled reactors were used. The reactors reviewed had volumes up to 250 L. These reactors were called multiple-frequency cells. They are installed with different transducers generating multiple frequencies. This flow-cell configuration makes it possible to change frequencies in the reactor. In Figure 9, a drawing of this kind of reactor is shown. There's seen that the configuration is showing two different frequencies (25 and 40 kHz) that can be applied on a different location in the reactor. This makes it possible to take advantage of the physical (20 kHz) and chemical (>200 kHz) properties of US in the same reactor. This kind of configuration can be used as flow-cell or even as a batch-system. (Gogate and Patil, 2016; Tiong et al., 2017)

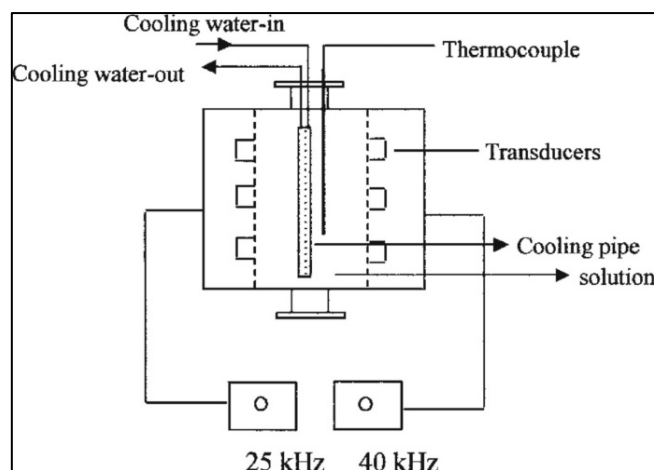


Figure 9: Configuration of a multiple-frequency reactor, used from Gogate and Patil (2016)

2.4.5 Operating temperature and pressure

For most of the experiments done in the literature, reactor temperatures around 20 °C or lower were used (Camargo-Perea et al., 2021; Henglein and Kormann, 1985; Merouani et al., 2015b; Naidu et al., 1994; Yasui, 2001). The bulk temperature will increase by time because of the very high temperatures that occur inside the bubble (even though it is very local). Due to the increase of bulk temperature, vapor pressure of water will increase which means more water vapor will be trapped inside the bubbles, gaining a higher production of free radicals. On the other hand, when temperature increases too much (higher than 25-30 °C), the collapse will be less violent, leading to lower temperatures inside the bubble. The decrease in temperature is due to the decrease of the value of γ (C_p/C_v). When lower temperatures and pressures occur, chemical yield of hydroxyl radicals and other reactive species will decrease.

The operating pressure is most of the time kept at atmospheric pressure. Because of the minor increase of efficiency and chemical yield when applying more pressure, not so many investigations were done in the past (Gogate and Patil, 2016).

2.5 Ultrasonic pharmaceutical removal

The removal of pharmaceutical compounds in wastewaters will be more important looking to the near future, to protect nature and human. A study of the World Health Organisation (WHO) published in 2011 showed that several pharmaceuticals were detected in surface and drinking water. The pharmaceutical concentrations were less than $0,1 \mu\text{g L}^{-1}$ but it is sure that some common pharmaceuticals as ibuprofen and bezafibrate (a cardiovascular drug) are present in water streams. The last years, the interest of use of AOP for pharmaceutical removal increased in the last 10 years. Regarding to data from SCOPUS, the publications are increased from 692 publications in 2010 to 2554 publications in 2020. The evolution is also showed in Figure 10.

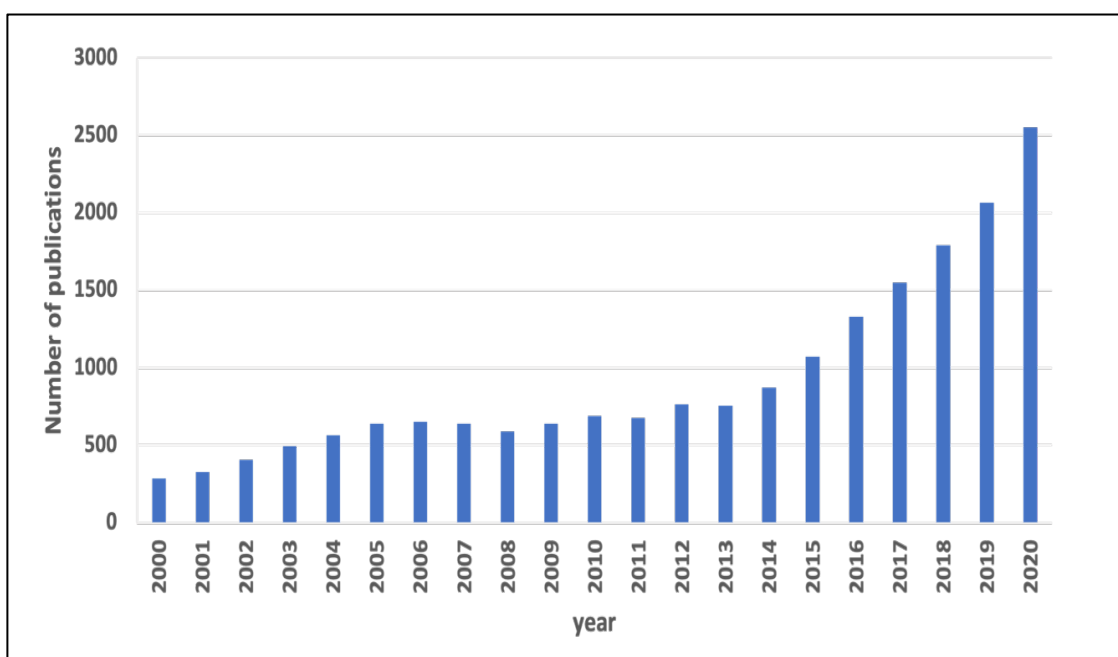


Figure 10: The evolution of publications on AOP's for pharmaceutical degradation (obtained with data from SCOPUS, search: "AOPs AND pharmaceuticals", all subjects)

Some recent research showed that it is possible to decompose some common pharmaceuticals only using US irradiated in the solution. Kanakaraju et al. (2018) reported an overview of different AOP's for specific pharmaceuticals. For sonolysis they found the following pharmaceuticals: ciprofloxacin, Diclofenac, Carbamazepine, Ibuprofen and Oxacillin. Some of these pharmaceuticals, especially Diclofenac, were found in wastewaters and surface waters over the world (Camargo-Perea et al., 2021; Kanakaraju et al., 2018). Most of the reported experiments, were done with deionized, milli-Q or ultrapure water. So, this can indicate that when matrix becomes more complex, efficiencies decrease heavily.

Looking to recent studies performed, a multi-frequency reactor was used by Camargo-Perea et al. (2021) for degradation of pharmaceuticals using only US. Mousally et al. (2019) used for their research a batch reactor as shown in Figure 11.

As mentioned earlier, the hydrophilic/hydrophobic properties of the pharmaceuticals are important in the reaction mechanism. The understanding of this property is important when investigating the reaction mechanisms. In a review study of Torres-Palma and Serna-Galvis (2018) they also confirm that the hydrophobic pharmaceuticals are more easily sonochemically removed compared to the hydrophilic pharmaceuticals. Furthermore, there is no dynamic model found in the literature which can give a proper vision of the occurring reactions inside these processes.

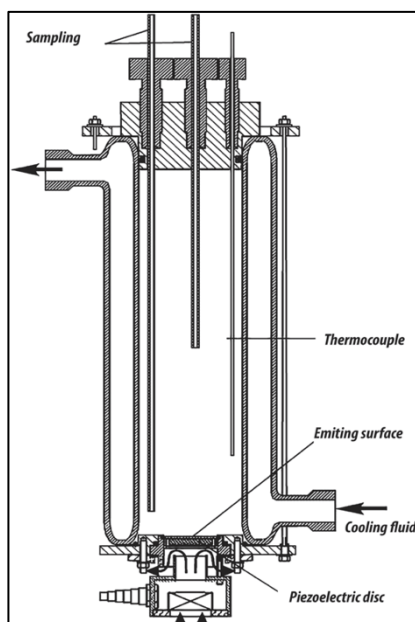


Figure 11: scheme of a sonochemical batch reactor with cooling jacket, used from Mousally et al. (2019)

2.6 Objectives

The aim of this master thesis is to obtain a chemical model which describes the chemical kinetics in the aqueous phase for US treatment of pharmaceuticals. Since there is no kinetical description for the radical production by ultrasound in the aqueous phase, the first step will be to find a suitable model to describe the reactions occurring in pure water. Secondly, the model will be calibrated and optimised using experimental data from the University of Antioquia Colombia. The last step will be to extend the model for pharmaceutical removal.

CHAPTER 3: MATERIALS AND METHODS

3.1 Introduction

In this chapter the used materials and techniques will be discussed. Describing radical chemistry is difficult because of the short existing time of the radical species. Because of these small existing times, it is difficult to detect radical species in general, so scientists must rely on kinetical studies to create a model. Simulation of these models can give a good estimation of what happens inside the reactor. In this work, simulations are used to determine the change of concentration of the radical species in the aqueous phase of an US reactor. The simulations are carried out with the program KPP, the kinetic pre-processor. The simulations can be calibrated by using experimental data for the concentration of hydrogen peroxide (H_2O_2) and the pH.

3.2 The Kinetic Pre-Processor (KPP)

To build a dynamic model, the program KPP or Kinetic Pre-Processor was used. KPP is developed by professor A. Sandu (Department of Computer Science Virginia Polytechnic Institute and State University Blacksburg, Virginia) and doctor R. Sander (Air Chemistry Department Max-Planck Institute of Chemistry, Mainz). A very detailed description of the program and the kinetic problem is published in 2002 (Damian et al., 2002). The program makes it possible to generate a code (C, Matlab or Fortran) that include all the ODE, only inserting the reactions, the reaction rate constants for each reaction and the initial concentrations. KPP was successfully used in chemical mechanisms from atmospheric tropospheric and stratospheric chemistry. Although KPP software is designed to solve atmospheric kinetic problems. Until now no kinetic problems in aqueous phase have been solved by the authors or other users. Regarding to this work no problems are detected for using the system for aqueous solution.

The install files and install guide can be found using the following link: <https://people.cs.vt.edu/asandu/Software/Kpp/>.

If the user is not familiar with installation of these kinds of programs or using Linux in general, an easy to follow step-by-step instructions are found in this link: <https://tomchor.github.io/ezkpp/README.html>.

3.2.1 Syntax rules

To understand the program, first it is important to know the syntax of the codes. KPP only works on Linux OS, or you can use a virtual box for Windows to run the system. As such, the system itself has no interface and works fully in the terminal of Linux. This means a basic knowledge of Linux commands are recommended.

Every command is written in capitals and begins with "#". When you want to write additional things like reaction circumstances or reaction numbers, you can use "{}". These are ignored by the system. If you want the system to ignore a line, double slash ("/") can be used in the beginning of the line. For some files a specific use of ":" and ";" are needed. The use of these will be explained in the subsection itself. Any name that is given by the user to a species or atom has to be less than 32 characters only containing numbers, letters or underscores. The first character always has to be a letter.

To generate a code, four input files are needed: a kpp file (.kpp) (I), a chemical description or also called definition file (.def) (II), a species file (.spc) (III) and an equation file (.eqn) (IV). To have a better understanding of the simulation program and to be able to understand the used codes in this thesis, a detailed (but easy to understand) description of each of the four files will be given in the next sections.

3.2.2 Species file (Root.spc)

The species file contains all the species that are listed in the equation file using an atom file that contains the elements that will be used. So, every Root.spc file starts with "#INCLUDE atom file". Then, each specie must be defined in one of three classifications. When the concentration of the specie does not change in the reaction (for example, water) it is defined as a fixed specie(#DEFFIX). When the concentrations change during time, it can be classified as variable (#DEFVAR) or, if the species react very fast like radicals, they must be defined as radicals (#DEFRAD). The species are defined under the classifications where they belong.

Defining a species is obtained by first give a definition for the species to insert in the equation file followed by a "=" and after that the molecules are summed up, ending with a ";". To give an example, water (H₂O) can be defined as showed in Figure 12:

```
#INCLUDE atoms

#DEFFIX
H2O   = H + O + O   ; {water, solvent}

#DEFVAR
H2O2  = 2 H + 2 O   ; {hydrogen peroxide}

#DEFRAD
HOR   = H + O       ; {hydroxyl radical}
HR    = H            ; {hydrogen radical}
```

Figure 12: Example of the chemical species file (Root.spc)

For species that can't be defined because there is a physical term like radiation, can be defined by using the command IGNORE. The same function can be used for reactions with organic matter where the composition of it is difficult to define or unknown.

3.2.3 Equation file (Root.eqn)

The chemical equation file starts with the command #EQUATIONS and is followed by the chemical equations, written like a chemist would write them, only using the already defined species in the Root.spc file. For some reactions, a stoichiometric value for the products is necessary. For that reason, the system is designed that it is possible to use stoichiometric values.

To generate the set of ODE's the reaction rate constant k of each reaction is needed. KPP makes it possible to insert the reaction rate constant value or use a function to define the rate constant as a function of temperature (Arrhenius equation) or for other reasons. The functions should be defined in the Root.def file. An example of the equation file, using the species defined in Figure 12 is showed in Figure 13.

```
#EQUATIONS
{1}   HOR + HOR =      H2O2 : 4.00E+9;
{2}   HOR + HR  =      H2O  : 7.00E+7;
```

Figure 13: Example of the equation file (Root.eqn)

The kpp language is also very clear in the figure. The equation itself ends with “:”, followed by the reaction rate constant or rate constant function and ends with “;”.

3.2.4 Definition file (Root.def)

The definition file, or kinetic description file, contains a lot of detailed information of the chemical model including the atoms, chemical species and used functions in the system. The definition file can be divided in several pieces. The Root.def file always starts with the inclusion of the species (Root.spc) and the equations (Root.eqn) using the command #INCLUDE. After the first two lines, some commands can be inserted regarding to mass balance, monitoring and data output. KPP makes it possible to check the mass balance of each reaction. This can be done with function #CHECK followed by the species that you want to check or when the user wants to check all species, use #CHECKALL.

To obtain the data of the wished species, the command #LOOKAT can be used. This function tells the program which data it should take up into the datafile. Also #LOOKATALL is an option to obtain the data from all species. The #MONITOR function just includes the species that the user wants to be displayed in a graph. For some unknown reason, the maximum to monitor species is 8.

After the command section, the initial conditions are next. The section starts with the command #INITVALUES followed by the initial concentrations of the species. The species need to be written as defined in the Root.spc section. If a lot of species have the same concentration, let's say zero, the command “ALL_SPEC = 0;” can be used. If concentration of other species is defined in the initial values section, the value will be considered, only the ones that aren't in the list will have an initial concentration of zero. Last, a conversion factor can be used when concentrations are in other dimensions by using “CFACTOR”.

All the above-described parts of the description file are displayed in Figure 14. Again, the species and reactions as described in the sections ... and ... is used. As showed in the figure, the syntax is similar to the species one. After the commands #LOOKAT, #CHECK and #MONITOR the species are listed separated by a “;”.

```
#INCLUDE Root.spc
#INCLUDE Root.eqn

#LOOKATALL
#CHECKALL
#MONITOR  HOR; HR; H2O2;

#INITVALUES
CFACTOR = 1.0      ;
HOR      = 1.0E-6  ;
HR       = 1.5E-8  ;
H2O     = 55.54   ;
```

Figure 14: Chemical description file example (Root.def)

After the first part, several program fragments can be inserted. The program fragments always begin on a new line with #INLINE and ends with #ENDINLINE. The code in between the two commands must be written in the target code, which in this case is Matlab code. The inserted information is placed in the right place by KPP which is determined by the type of the inline code. There are five different inline types that can be used. The types are listed in Table 3. The type of inline is selected by writing after the #INLINE LANGUAGE(F90/F77/C/MATLAB)_type. In the table and further description, MATLAB_type is indicated as only Matlab is used in this work.

Table 3: Inline types

| <i>Inline type</i> | <i>File placement</i> | <i>Description</i> |
|----------------------|-----------------------|-----------------------------------------------------------------------------------------|
| <i>MATLAB_GLOBAL</i> | Root_Global_defs.m | Declare global variables |
| <i>MATLAB_INIT</i> | Root_Initialize.m | Define initial values before integration |
| <i>MATLAB_RATES</i> | Root_Rates.m | New subroutines to calculate rate coefficients |
| <i>MATLAB_RCONST</i> | Root_Rates.m | Define time-dependent values of rate coefficients that were declared with MATLAB_GLOBAL |
| <i>MATLAB_UTIL</i> | Root_Util.m | Define utility subroutines |

The most important types in this work, will be the MATLAB_INIT, MATLAB_RATES and the MATLAB_GLOBAL inline codes. In the INIT-type all variables are defined as the parameters for the Rosenbrock integrator (will be explained later), integration time, absolute and relative tolerance and other parameters. In the RATES-type section, functions that describe the reaction rate constants that are used in the equations are inserted. The GLOBAL type can be used just to insert some global variables that the user may need. To have a better understanding of the text, an example of the used inline codes in this work is showed in Figure 15.

```
#INLINE MATLAB_GLOBAL
global RCNTRL ICNTRL POWER
#ENDINLINE

#INLINE MATLAB_INIT
global TSTART TEND DT TEMP RTOLS ATOLS RCNTRL ICNTRL POWER
TSTART = 0.0;
RCNTRL = [0 1e-10 0 0.2 6 0.1 0.9];
ICNTRL = [1 0 0 0];
TEND = 1200;
DT = 1e-10;
TEMP = 298.15;
RTOLS = 1.0E-13;
ATOLS = 1.0E-13;
POWER = 4.15e-8;
#ENDINLINE

#INLINE MATLAB_RATES
function [rate]=SonoSource()
global TIME POWER;
if(TIME<=3600)
    rate=POWER;
else
    rate=0.0;
end
return
#ENDINLINE
```

Figure 15: Inline codes examples in the description file (Root.def)

3.2.5 Kpp file (Root.kpp)

The kpp file is the file that includes all the commands to generate the code. Depending on the application, the files can be different. To give a proper overview of the settings used for the simulations carried out in this thesis the following code will be described:

```
#MODEL      sonolysistest
#INTEGRATOR  none
#INTFILE     Rosenbrock
#LANGUAGE    Matlab
#DRIVER      rosendrv
#JACOBIAN    SPARSE_LU_ROW
#HESSIAN     on
#STOICMAT    on
```

Figure 16: Root.kpp file example

The #MODEL is the command that defines the model. Every file that is made and that will be generated will have this name. For the integration method two ways paths are available. It is possible to use the integrators inside the KPP-system itself or using self-made or modified files. When using pre-installed integrators, the integrator name must be defined in function #INTEGRATOR. When using an integrator-file not pre-installed, #INTEGRATOR is set as none and the function #INTFILE defines the integration-file that will be used.

KPP is able to generate different output codes, depending on the computer language that is requested. The languages available are Fortran 90, Fortran7, C and Matlab and can be used using function #LANGUAGE.

The driver-file (function #DRIVER) is responsible for creating the necessary files by calling the integration routine and reading the datafiles. When using a different integrator or integration-file, it can happen that the driver needs to be changed as well. In the code shown in figure 12, there is a driver specially for using Rosenbrock integration methods (rosendrv).

The #JACOBIAN function is used to indicate how you want to use the Jacobian for the integration. It is possible to switch it OFF, use it FULL (square matrix) or you can use a Jacobian in sparse with SPARSE_ROW or SPARSE_LU_ROW.

There are even some more functions that you can switch on or off depending on the needs of the model. The ones described above are the most used ones. In total there are 19 different functions which are well described in the manual of KPP if needed.

3.2.6 Numerical method

KPP contains a lot of different numerical methods to use if very stiff ODE's appear. As the obtained ODE's can be classified as stiff ODE's these methods are very useful. The most used ones are the Rosenbrock and Sdirk (Runge Kutta) methods. For this work, Rosenbrock integrations worked well enough to get representative simulation results. They belong to a series of methods which avoid non-linear systems by replacing it by a sequence of linear systems. Therefore, these methods are called "linearly implicit Runge Kutta methods".

With Rosenbrock methods, the non-linear system is avoided completely and is the easiest to program method for stiff ODE. The mathematical side of the method is not described in this work but can be found in section IV.7 of the book Solving Ordinary Differential Equations II (Hairer and Wanner, 1996).

3.2.7 Generated codes

With the four files (Root.def, Root.spc, Root.eqn and Root.kpp) kpp can compile the necessary files in the chosen codes. In this work, Matlab codes (*.m) were used. In Table 4 all the generated files are displayed. The ones that are most valuable are indicated bold and will be described more in detail under the table. Some codes that are generated don't have any function regarding to this work and will be indicated with a strikethrough.

Table 4: List of the generated Matlab files

| <i>File</i> | <i>Description</i> |
|-------------------------------------------|--------------------------------------------------------------|
| Root_main.m | Driver |
| Root_Fun.m | ODE functions |
| <i>Root_Fun_Chem.m</i> | Template for ODE function |
| <i>Root_Parameters.m</i> | Parameters |
| <i>Root_Global_defs.m</i> | Definition of the variables |
| Root_Monitor.m | Monitor variables |
| <i>Root_Sparse.m</i> | Sparsity data |
| <i>Root_Jac_SP.m</i> | ODE Jacobian in sparse format |
| <i>Root_Jac_Chem.m</i> | Template for the ODE Jacobian |
| <i>Root_JacobianSP.m</i> | Sparsity data structure |
| <i>Root_Hessian.m</i> | ODE Hessian in sparse format |
| <i>Root_HessianSP.m</i> | Sparsity data structures |
| <i>Root_HessTR_Vec.m</i> | Hessian action on vectors |
| <i>Root_Hess_Vec.m</i> | Transposed Hessian action on vectors |
| <i>Root_stoichiom.m</i> | Derivatives of Fun and Jac with respect to rate coefficients |
| <i>Root_StoiciomSP.m</i> | Sparse data |
| <i>Root_ReactantProd.m</i> | Reaction products |
| <i>Root_JacReactantProd.m</i> | Jacobian of the reaction products |
| Root_Rates.m | User defined reaction rate laws |
| <i>Root_Util.m</i> | Utility In/output, creates data file |
| <i>Root_Update_PHOTO.m</i> | Photolysis rate constants |
| Root_Update_RCONST.m | All the reaction rate constants |
| <i>Root_Update_SUN.m</i> | Solar intensity function |
| <i>Root_GetMass.m</i> | Checks the mass balance for selected values |
| Root_Initialize.m | Set initial values |
| <i>Root_Shuffle_kpp2user.m</i> | Shuffle concentration vector |
| <i>Root_Shuffle_user2kpp.m</i> | Shuffle concentration vector |

3.2.7.1 *Root_Main.m*

The main file contains all the information and Matlab commands to obtain the concentration profiles of the wished species. The file is more specifically, the representation of the driver after modification by the substitution pre-processor. The driver is selected, as mentioned earlier, in the Root.kpp file (#DRIVER).

3.2.7.2 *Root_Fun.m*

In this file, all the ODE's are displayed. First, for each reaction the reaction rate A is calculated. Regarding if the concentration of the species is fixed or variable, it is indicated with F(x) or V(x) respectively. Then Vdot(x) of each species is computed. Vdot is the vector that describes the time derivative of the variable species. The x between the hooks is a number that is given to define each specie. The numbers connected with each species can be found in the Root_Monitor.m file.

3.2.7.3 *Root_Monitor.m*

The monitor file contains information about the chemical species and the reactions where they are in evolved. All species and reactions are linked to a number starting from 1. The linked number is used in other several codes to indicate the species or reaction. This file also displays the commands #MONITOR and #CHECK from the definition file (Root.def).

3.2.7.4 *Root_Rates.m and Root_Update_RCONST.m*

As the file 'rates' tells itself, the rates file includes all the reaction rate constant functions that are included in the system (Arrhenius and SUN function) and functions inserted by the user which are specified in the Root.def file. The Update_RCONST file is basically the same file. Only difference is that the constants itself are defined to use in the ODE's. This is indicated as: RCONST(x)= function, with x the number of the reaction.

3.2.7.5 *Root_Initialize.m*

The initialize contains a lot of information as the initial conditions, all the reaction rate constants (Rconst(x)=..., with x the number of the reaction), the user's reaction rate constant functions and some variables that were pre-defined in the Root.def file. The file includes everything that is defined under the #INLINE MATLAB_INIT part in the Root.def file.

3.3 US experiments

The present TFM is carried out under the framework of a collaboration with the Grupo de Investigación en Remediación Ambiental y Biocatálisis (GIRAB) de la Universidad de Antioquia (Medellín, Colombia). The experimental methods are briefly described in this section using publications of their research (Camargo-Perea et al., 2021) and were published in this work with permission of the researchers (Professor Torres-Palma and Doctor Serna-Galvis).

3.3.1 Reactor

The experiments were done using a Meinhardt multifrequency laboratory reactor (500 mL) (<https://www.meinhardt-ultrasonics.com>) cooled with a cooling jacket using Huber Minichiller (<https://www.huber-online.com/en/index.aspx>). The temperature was kept at 20 ± 2 °C. The data used in this work to compare were obtained from experiments using 250 mL of reaction volume, an operating frequency of 375 kHz and reaction times between 20 minutes and 2.5 hours. The reactor and the cooling circuit is showed in Figure 17.



Figure 17: US reactor with cooling jacketed, with permission of E. Serna-Galvis

Experiments were carried out in pure water (distilled) and distilled water containing pharmaceuticals. The pharmaceuticals used for calibration of the model were ACE (acetaminophen) and CIP (Ciprofloxacin). ACE is sold under the name of Paracetamol, CIP is an antibiotic known under the commercial names of Ciproxin, Cipro and Ciprobay.

3.3.2 Chemical analysis

At several times during the sonication, samples were withdrawn from the chemical reactor for chemical analysis. The key parameters to analyse when performing sonolysis of pure water is the pH and the hydrogen peroxide concentration. For the analysis of the hydrogen peroxide, iodometry method was used with spectrophotometry detection. For the analysis, samples of the 600 μL experimental solution were taken and mixed in a quartz cell containing 1350 μL of potassium iodide (0.1 M) and 50 μL of an ammonium heptamolybdate (0.01 M) solution. After 5 minutes of reaction, the quartz cell was placed in a Mettler Toledo UV5 spectrophotometer, and the absorbance was measured at 350 nm.

Besides the experiments in pure water, other experiments were carried out with some pharmaceuticals. The pH was measured using a pH93 probe. The pharmaceuticals were analysed using a Thermo Scientific Dionex UltiMate 3000 UHPLC apparatus, equipped with an Acclaim™ 120 RP C18 column (5 μm , 4.6 \times 150 mm) and a diode array detector. In the mobile phase, the formic acid solution was used at 10 mM and pH 3.0. In the following table (Table 5) the chromatographic details for each of the used pharmaceuticals is showed.

Table 5: Chromatographic details for ACE and CIP

| <i>Pharmaceutical</i> | <i>Detection wavelength (nm)</i> | <i>Mobile phase Formic acid/Acetonitrile (%v/%v)</i> | <i>Retention time (min)</i> |
|-----------------------|----------------------------------|------------------------------------------------------|-----------------------------|
| <i>ACE</i> | 243 | 85/15 | 7.0 |
| <i>CIP</i> | 280 | 85/15 | 9.8 |

CHAPTER 4: CHEMICAL MODEL

4.1 Introduction

The production of the radicals is due to the US waves and takes place in a different phase, the gas phase. Because of the extreme conditions inside the bubble in terms of temperatures and pressures, it makes the description of the kinetics complex. Also, mass transfer effects are occurring at the interface of the cavitation bubbles which makes it even more complex to describe the kinetics. Merouani and co-workers (Merouani et al., 2015a) proposed the semi-empirical formula 2.6 to calculate the number of bubbles inside the reactor. With the number of bubbles, an estimation of the kinetics could be made using ODE's that are equal to equation 2.11.

$$N = \frac{r_{H_2O_2}}{n_{H_2O_2}^{0.5}(n_{OH\cdot} + n_{HO_2\cdot})} \quad (2.6)$$

$$\frac{dc_i}{dt} = N \cdot n_i + \sum_j R_{ij}(T, c) = f(T, c) \quad i = 1, \dots, n, \quad j = 1, \dots, r. \quad (2.11)$$

Nevertheless, using this method of prediction needs a lot of time and different systems are needed to calculate the bubble radius, the amount of moles for the species generated inside the bubble and experiments for the reaction rate of hydrogen peroxide. Still, in this work another approach for the aqueous reactions is proposed only looking to the aqueous phase in the first place.

4.2 Mass transfer

In sonochemistry the phenomena of mass transfer cannot be ignored. In literature, mass transfer in sonochemistry is not well described due to the non-linear oscillations of the bubbles. In general, the mass transfer of a component from the gas to the liquid phase can be described as showed in Figure 18.

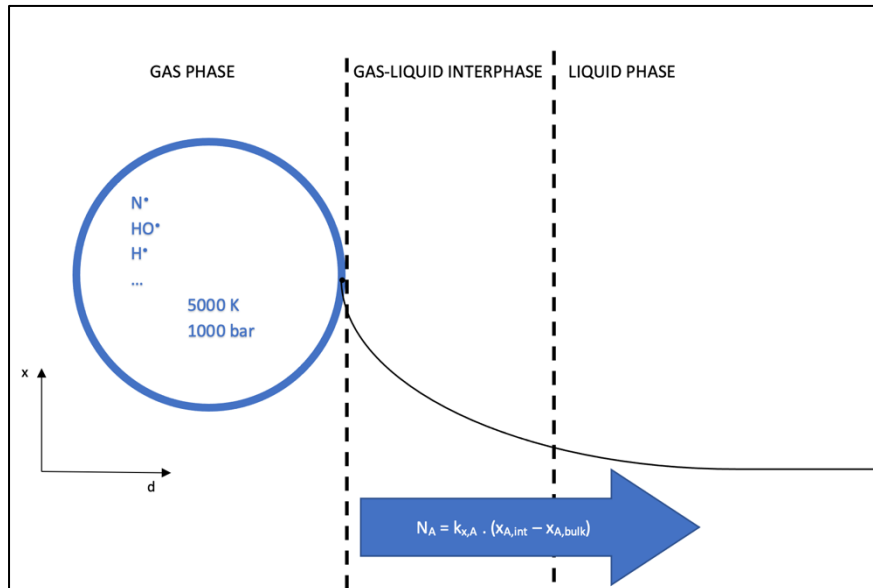


Figure 18: Mass transfer of a component A from gas to liquid phase

The mass flow N of component A is proportional to the difference in fraction of the component in the bubble and in the bulk solution:

$$N_A = k_x(x_{A,int} - x_{A,bulk}) \quad (4.1)$$

The total mass flux for one component A from the cavitation bubble to the liquid can be described by the following formula:

$$J_A = N_A \cdot n_b \cdot \alpha \quad (4.2)$$

With J_A the total flux in mole/s, N_A the mass flow rate in mole/m².s, n_b the number of bubbles in the reactor and α is the exchange surface for each bubble.

The mass transfer of each substance can be defined by a source term Φ . This term is assumed to be equal to the total mass flux divided by the reactor volume.

$$\Phi = \frac{J_A}{V_{reactor}} \quad [\text{M} \cdot \text{s}] \quad (4.3)$$

Considering spherical bubbles, the total production rate for these substances can be equal to:

$$\Phi = \frac{n_b}{V_{reactor}} 4 \cdot \pi R_b^2 \cdot k_{x,A} \cdot (x_{A,int} - x_{A,bulk}) \quad (4.4)$$

Or when working with concentrations:

$$\Phi = \frac{n_b}{V_{reactor}} 4 \cdot \pi R_b^2 C_T \cdot k_{L,A} \cdot (C_{A,int} - C_{A,bulk}) \quad (4.5)$$

Where C_T is the molar density of the solvent (mole/m³), R_b is the radius of the bubble (m), $k_{L,A}$ is the mass transfer coefficient for component A with concentrations expressed in (mole/m³) and $C_{A,int}$ and $C_{A,bulk}$ are the concentrations at the interphase and liquid bulk phase respectively (mole/m³).

Some of the values from equation 4.5 are available in literature or can be obtained by experimental results. Also, it is possible to assume that the fraction of radical species are close to zero in the bulk phase due to the low concentrations and fast reaction times and therefore negligible.

$$x_{A,bulk} = C_{A,bulk} = 0 \quad (4.6)$$

Therefore, the fraction at the interface can be related to the Henry's law:

$$x_{A,int} = H_A \cdot y_{Ai} \quad (4.7)$$

With y_{Ai} is the molar liquid fraction of component A at the gas-liquid interphase.

Equation 4.4 can now be rewritten as:

$$\Phi = n_g \cdot \pi \cdot D_b^2 \cdot k_x \cdot H_A \cdot y_{Ai} \quad (4.8)$$

Or when working with concentrations:

$$\Phi = n_g \cdot \pi \cdot D_b^2 \cdot k_L \cdot C_T H_A \cdot y_{Ai} \quad (4.9)$$

With n_g as the bubble density ($n_b/V_{reactor}$) in bubbles/m³. This value for bubble density is correlated to the acoustic power transmitted through the vessel. The bubble diameter is also correlated to the acoustic power and the frequency applied. As noticed in the literature review, the diameter is estimated to be around 7 μm when using 300 kHz waves.

For the determination of the mass transfer coefficient, the known expressions for a single spherical bubble can be used using dimensionless expressions as Reynolds, Schmitz and Sherwood numbers. Using Sherwood numbers, the mass transfer coefficient can be found in various ways like for example:

$$Sh = 2 + 0.6 Re^{\frac{1}{2}} \cdot Sc^{1/3} \quad (4.10)$$

$$Sh = \frac{k_L \cdot D_b}{D} \quad (4.11)$$

With D as the diffusivity coefficient.

The Reynolds and Schmitz number are equal to:

$$Re = \frac{\rho_l \cdot D_b \cdot v}{\mu_l} ; Sc = \frac{\mu_l}{\rho_l \cdot D} \quad (4.12)$$

With ρ_l as the liquid density, μ_l as the dynamic viscosity and v as the relative velocity of the liquid. This last one is maybe the only unknown variable. As a first approach, the bubble wall velocity could be a good option.

Finally, the concentrations inside the bubble can be predicted by using simulations. These results are described in the next section. Using the molar fractions of each substance the above-described method can be used to predict the mass transfer to the liquid phase. Considering no mass transport limitations inside the cavitation bubble the molar fraction of A at interface is equal to the fraction in the bulk.

$$y_{Ai} = y_{Ab} \quad (4.13)$$

Although this source term Φ is proportional to y_{Ab} the other property constants cannot be very easy evaluated. For now, there is assumed that each component transfers 100 % from the gas to the liquid phase without any mass transfer limitations. Possibly, in a further state of research, a more precise and personalised approach for each component will be needed.

From now, the source term Φ is used to describe the source reaction.

4.3 Proposal of the model for US radiation in water

The first step was to solve the radical production problem and create a model for the reactions that are occurring in pure water. First, research in literature was necessary to find similar models or simulation tests regarding cavitation bubbles. In literature, two main references are used for the radical generation: Merouani et al. and Yasui (et al.). Both researchers have multiple papers coupling the bubble dynamics to the chemical kinetics inside a single the cavitation bubble. Merouani et al. used oxygen saturated water and an operating frequency of 355 kHz, compared to Yasui et al. who used air saturated water simulations at an operating frequency of 300 kHz. Both simulations are in line with the frequencies used for the removal of pharmaceuticals so that's why these two simulations were used.

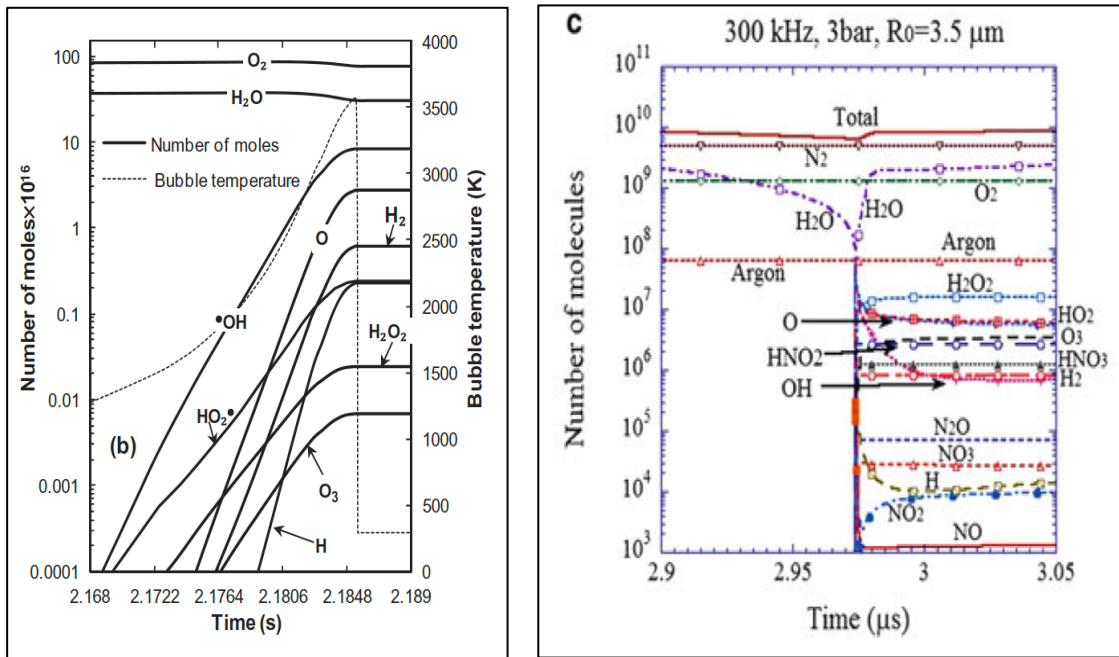


Figure 19: Numerical simulations of (left) Merouani et al. (2015b) using 355 kHz in oxygen atmosphere and (right) Yasui et al. (2007) using 300 kHz in air atmosphere

In both figures, steady state concentration of the species is obtained. Something that arises comparing the two profiles is that the amount of hydrogen peroxide produced in an oxygen bubble (Merouani et al., 2015c) is way lower compared to the air bubble (Yasui et al., 2007). This can be because both references used different chemical models. Also, both used different physical parameters which can affect the outcome in a very big way.

Using the figures described above, it is possible to calculate an estimated fraction for all the reactive species produced in the cavitation bubbles. Using these fractions, it is possible to create a “source reaction”. The reaction rate constant of this reaction can then in turn be described by a function that is correlated with the frequency and acoustic amplitude. The function which describes the reaction rate constant is just a step function that has a magnitude POWER. The function is showed in equation 4.14.

$$if \left\{ \begin{array}{l} x \leq t \rightarrow k = POWER \\ x > t \rightarrow k = 0 \end{array} \right\} \quad (4.14)$$

with t the time of US radiation, k the reaction rate constant and POWER a magnitude correlated to the physical properties of the US. With this easy function, it was possible to simulate what happens when irradiating for a long or short period and what happens after radiation with the reactive species.

In a further stadium, it can also be useful to use a pulse like process. By switching on and off the US source, a lower energy consumption can be obtained, still generating enough radicals to react. Because of that, a second function was introduced to describe a pulsating ultrasound source. This function was implemented in Matlab using the command "impulsetrain" and is showed in

Figure 20. The variables TIME, TAU, DELTA and CN are the time of integration, the time that radiation is on, time that radiation is off and the number of pulse cycles respectively. This code was also used to describe the first function in equation 4.14, using the value CN = 1.

```
function [rate]=SonoSource()
global TIME POWER TAU DELTA CN;
rate=POWER*impulsetrain(TIME,TAU,DELTA ,CN);
return

function y=impulsetrain(t,tau,delta,nc)
period=tau+delta;
ncy=floor(t/period);
tp=(t-ncy*period).*(ncy<nc)+(tau+delta/2).*(ncy>=nc);
y=heaviside(tp)-heaviside(tp-tau);
return
```

Figure 20: Matlab code for the impulse function

The following sections will go deeper into the models created using Merouani's and Yasui's information obtained from their publications (Merouani et al., 2015c, 2015c; Yasui, 2018, 2016; Yasui et al., 2008).

4.3.1 Based on Merouani

The model was first created using oxygen saturated water (Meroauni et al. results). In this case, only oxygen and hydrogen related radicals are produced. Using Figure 21, fraction of each of the species were determined by assuming that for all the species created inside the bubble, the same fractions are transferred from the gas phase to the liquid phase. The calculated fractions are showed in Table 6.

Calculation example:

The total absolute numbers of moles are approximately:
 $9 + 2.8 + 0.63 + (2 \times 0.21) + 0.022 + 0.007 = 12.879$ units

Fractions can then be calculated as followed:

$$\alpha_{OH} = \frac{9}{12.879} = 0.6988 \quad (4.15)$$

There must be noticed that the presence of oxygen and water is ignored in the calculations of the fractions due to their almost constant concentration and low reactivity.

Table 6: Fractions of the species obtained from numerical simulations of Merouani et al. (2015b)

| Specie | Fraction (-) |
|-------------|--------------|
| $\cdot OH$ | 0.6988 |
| $O\cdot$ | 0.2174 |
| H_2 | 0.0489 |
| $HO_2\cdot$ | 0.0163 |
| $H\cdot$ | 0.0163 |
| H_2O_2 | 0.0017 |
| O_3 | 0.00053 |

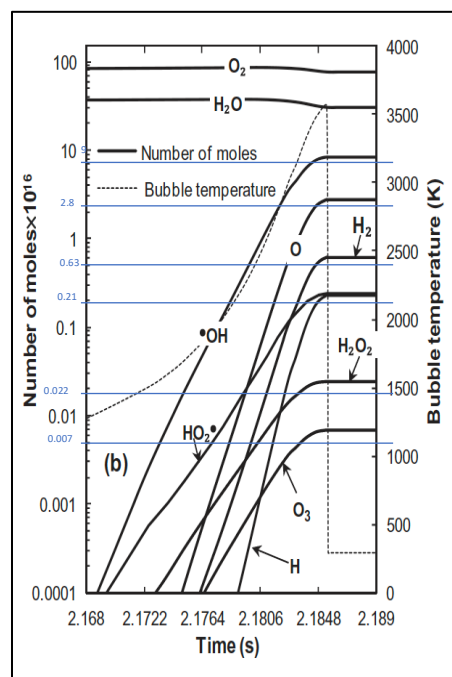


Figure 21: The use of the numerical simulations of Merouani et al. (2015b) to determine the fraction of each species in the bubble

Finally, the source reaction can be described as using the fractions of the species as a stoichiometric value:



Using this reaction as a reaction to describe the creation of the reactive species due to the US radiation, a model was created using several references regarding radical chemistry in aqueous solutions (Beltrán, 2004; Burkholder et al., 2019; Buxton et al., 1988, 1988; Ershov and Gordeev, 2008; Gonzalez and Mártire, 1997; Mizuno et al., 2007). The complete model is showed in Table 7. The numbers of the reactions are in correlation with the numbers of reactions in the KPP code. This particular code, is attached at the end of this work in Appendix I.

Table 7: Reactions used in the chemical model for US radiation in oxygen saturated water

| Reaction | $k (M^{-1}.s^{-1})$ | References |
|--------------------------------------------------------------------------------------------------------------------------------------------------|-----------------------|------------------------------|
| US $\rightarrow 0.0163 H^{\bullet} + 0.6988 \cdot OH + 0.2174 O^{\bullet} + 0.0489 H_2 + 0.0163 HO_2^{\bullet} + 0.0017 H_2O_2 + 0.00053 O_3$ | Function | This work |
| 1 $\cdot OH + H_2O_2 \rightarrow HO_2^{\bullet} + H_2O$ | 2.00×10^7 | (Ross and Ross, 1977) |
| 2 $\cdot OH + HO_2^{\bullet} \rightarrow O_2^{\bullet-} + H_2O$ | 7.50×10^9 | (Burkholder et al., 2019) |
| 3 $O^{\bullet} + H_2O_2 \rightarrow O_2^{\bullet-} + H_2O$ | 5.00×10^8 | (Buxton et al., 1988) |
| 4 $O^{\bullet} + HO_2^{\bullet} \rightarrow O_2^{\bullet-} + H_2O$ | 4.00×10^8 | (Buxton et al., 1988) |
| 5 $\cdot OH + \cdot OH \rightarrow H_2O_2$ | 4.00×10^9 | (Ross and Ross, 1977) |
| 6 $\cdot OH + O^{\bullet} \rightarrow HO_2^{\bullet}$ | 2.00×10^{10} | (Buxton et al., 1988) |
| 7 $\cdot OH + HO_2^{\bullet} \rightarrow O_2 + H_2O$ | 1.00×10^{10} | (Burkholder et al., 2019) |
| 8 $\cdot OH + O_2^{\bullet-} \rightarrow O_2 + OH^{-}$ | 1.01×10^{10} | (Burkholder et al., 2019) |
| 9 $O^{\bullet} + O_2^{\bullet-} \rightarrow O_2 + 2 OH^{-}$ | 6.00×10^8 | (Ross and Ross, 1977) |
| 10 $O^{\bullet} + O_2 \rightarrow O_3^{\bullet-}$ | 3.60×10^9 | (Buxton et al., 1988) |
| 11 $O^{\bullet} (+ H_2O) \rightarrow \cdot OH + OH^{-}$ | 1.70×10^6 | (Buxton et al., 1988) |
| 12 $\cdot OH + OH^{-} \rightarrow H_2O + O^{\bullet}$ | 1.30×10^{10} | (Buxton et al., 1988) |
| 13 $HO_2^{\bullet} + HO_2^{\bullet} \rightarrow H_2O_2 + O_2$ | 3.10×10^6 | (Ross and Ross, 1977) |
| 14 $HO_2^{\bullet} + O_2^{\bullet-} \rightarrow O_2 + HO_2^{\bullet}$ | 1.00×10^8 | (Ross and Ross, 1977) |
| 15 $HO_2^{\bullet} + H_2O_2 \rightarrow O_2 + OH + H_2O$ | 0.5 | (Ross and Ross, 1977) |
| 16 $H_2O_2 + O_2^{\bullet-} \rightarrow O_2 + \cdot OH + OH^{-}$ | 0.13 | (Burkholder et al., 2019) |
| 17 $HO_2^{\bullet} \rightarrow H^{\bullet} + O_2^{\bullet-}$ | 7.00×10^5 | (Ershov and Gordeev, 2008) |
| 18 $H^{\bullet} + O_2^{\bullet-} \rightarrow HO_2^{\bullet}$ | 4.50×10^{10} | (Ershov and Gordeev, 2008) |
| 19 $H_2O_2 \rightarrow H^{\bullet} + HO_2^{\bullet}$ | 0.0356 | (Ershov and Gordeev, 2008) |
| 20 $H^{\bullet} + HO_2^{\bullet} \rightarrow H_2O_2$ | 2.00×10^{10} | (Ershov and Gordeev, 2008) |
| 21 $H_2O \rightarrow H^{\bullet} + OH^{-}$ | 2.50×10^{-5} | (Ershov and Gordeev, 2008) |
| 22 $H^{\bullet} + OH^{-} \rightarrow H_2O$ | 1.40×10^{11} | (Ershov and Gordeev, 2008) |
| 23 $O_3 + OH^{-} \rightarrow HO_2^{\bullet} + O_2$ | 48 | (Neta et al., 1988) |
| 24 $O_3 + OH^{-} \rightarrow HO_2^{\bullet} + O_2^{\bullet-}$ | 70 | (Neta et al., 1988) |
| 25 $O_3 + O_2^{\bullet-} \rightarrow O_3^{\bullet-} + O_2$ | 1.60×10^9 | (Gonzalez and Mártire, 1997) |
| 26 $O_3 + \cdot OH \rightarrow HO_2^{\bullet} + O_2$ | 1.80×10^8 | (Buxton et al., 1988) |
| 27 $O_3 + H_2O_2 \rightarrow HO_3^{\bullet}$ | 0.065 | (Mizuno et al., 2007) |
| 28 $O_3 + HO_2^{\bullet} \rightarrow O_3^{\bullet-} + HO_2^{\bullet}$ | 2.80×10^6 | (Bezbarua and Reckhow, 2004) |
| 29 $HO_3^{\bullet} \rightarrow \cdot OH + O_2$ | 1.10×10^5 | (Beltrán, 2004) |
| 30 $O_3^{\bullet-} \rightarrow O^{\bullet} + O_2$ | 7.00×10^8 | (Ross and Ross, 1977) |
| 31 $O_3^{\bullet-} + \cdot OH \rightarrow HO_2^{\bullet} + O_2^{\bullet-}$ | 8.50×10^9 | (Buxton et al., 1988) |
| 32 $O_3^{\bullet-} + O^{\bullet} \rightarrow 2 O_2^{\bullet-}$ | 7.00×10^8 | (Buxton et al., 1988) |
| 33 $H^{\bullet} + O_2 \rightarrow HO_2^{\bullet}$ | 2.00×10^{10} | (Burkholder et al., 2019) |
| 34 $HO_2^{\bullet} + H^{\bullet} \rightarrow H_2O_2$ | 1.00×10^{10} | (Buxton et al., 1988) |
| 35 $H^{\bullet} + O_2^{\bullet-} \rightarrow HO_2^{\bullet}$ | 2.00×10^{10} | (Buxton et al., 1988) |
| 36 $H^{\bullet} + H_2O_2 \rightarrow \cdot OH + H_2O$ | 9.00×10^7 | (Buxton et al., 1988) |
| 37 $H^{\bullet} + \cdot OH \rightarrow H_2O$ | 7.00×10^9 | (Buxton et al., 1988) |
| 38 $2 H^{\bullet} \rightarrow H_2$ | 7.75×10^9 | (Buxton et al., 1988) |
| 39 $H^{\bullet} (+ H_2O) \rightarrow \cdot OH + H_2$ | 9.00×10^7 | (Buxton et al., 1988) |
| 40 $O^{\bullet} (+ H_2O) \rightarrow 2 \cdot OH$ | 1.00×10^{10} | (Burkholder et al., 2019) |
| 51 $\cdot OH + H_2 \rightarrow H^{\bullet} + H_2O$ | 4.00×10^7 | (Burkholder et al., 2019) |
| 52 $O^{\bullet} + H_2 \rightarrow H^{\bullet} + \cdot OH$ | 8.00×10^7 | (Buxton et al., 1988) |
| 53 $O_3 + H^{\bullet} \rightarrow \cdot OH + H^{\bullet}$ | 3.80×10^{10} | (Neta et al., 1988) |

This model was then programmed in KPP, and simulations were done varying the time of reaction, time of US radiation and the source reaction "POWER" magnitude. The same model is used for the approach in air saturated water, with addition of nitrogen involving reactions. The resulting simulations will be described in detail in Chapter 5: Results and discussion.

4.3.2 Based on Yasui

For the air saturated model, the simulations of Yasui and co-workers were used (Yasui et al., 2007). The same principle of generation of a source reaction was applied to create a likely reaction as in the previous section. When sonofication takes place in an air environment, a different fraction of the species generated in the bubbles occurs. The method of determining the fractions is similar as the method used in Figure 21 using the data of Yasui et al. (2007), showed in Figure 22, the fractions are calculated in the same way regarding the previous model, not using the fraction of nitrogen, argon and water gas. The resulting fractions are displayed in Table 8.

Table 8: fractions of the species obtained from numerical simulations of Yasui et al. (2007)

| Specie | Fraction (-) |
|----------------|--------------|
| H_2O_2 | 0.49176 |
| HO_2^\bullet | 0.12941 |
| O^\bullet | 0.12941 |
| O_3 | 0.09835 |
| HNO_2 | 0.07765 |
| HNO_3 | 0.03106 |
| H_2 | 0.02071 |
| $^\bullet OH$ | 0.01812 |
| N_2O | 0.00207 |
| NO_3^\bullet | 0.00078 |
| H^\bullet | 0.00039 |

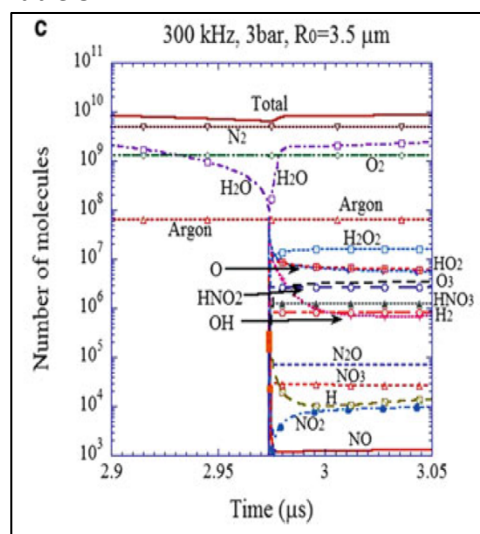
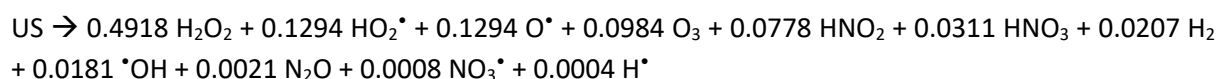


Figure 22: The used numerical simulations of Yasui et al. (2007) to determine the fractions of the generated species in an air bubble

Regarding to the information obtained from Yasui et al. it seems like their model gives a completely different outcome then the one of Merouani. The amount of hydrogen peroxide is way higher than the one in oxygen saturated water (0.0017). This gives an indication that the production of hydrogen peroxide in air saturated water will be more due to sonolytic production and not from the radical reactions. The source reaction can now be given as followed:



Using this reaction in the same way as the previous section, an extension of the model can be made including the new species formed because of the presence of air. The extension of the model showed in Table 7 are showed in Table 9. Some new references were needed to identify the additional reactions (Mack and Bolton, 1999; McKenzie et al., 2016).

Table 9: Reactions used in the chemical model for US radiation of air saturated water.

| Reaction | k ($M^{-1}.s^{-1}$) | References |
|---------------------------------------------------------------------------------------------------------------------------------------------------------------------------------------------------------------------------------------------------|-------------------------|-------------------------|
| ϕ US \rightarrow 0.4918 H_2O_2 + 0.1294 HO_2^{\bullet} + 0.1294 O^{\bullet} + 0.0984 O_3 + 0.0778 HNO_2 + 0.0311 HNO_3 + 0.0207 H_2 + 0.0181 $^{\bullet}OH$ + 0.0021 N_2O + 0.0008 NO_3^{\bullet} + 0.0004 H^{\bullet} | Function | This work |
| 41 $NO^{\bullet} + ^{\bullet}OH \rightarrow HNO_2$ | 1.00×10^{10} | (Mack and Bolton, 1999) |
| 42 $NO_2^- + ^{\bullet}OH \rightarrow NO_2^{\bullet} + OH^-$ | 1.00×10^{10} | (Mack and Bolton, 1999) |
| 43 $NO_2^{\bullet} + NO_2^- \rightarrow N_2O_3$ | 1.10×10^{10} | (Mack and Bolton, 1999) |
| 44 $N_2O_3 (+ H_2O) \rightarrow 2 HNO_2$ | 5.30×10^2 | (Mack and Bolton, 1999) |
| 45 $2 NO_2^{\bullet} \rightarrow N_2O_4$ | 4.50×10^8 | (Mack and Bolton, 1999) |
| 46 $N_2O_4 (+ H_2O) \rightarrow NO_2^- + 2 H^+ + NO_3^-$ | 1.00×10^3 | (Mack and Bolton, 1999) |
| 47 $H^{\bullet} + HNO_2 \rightarrow NO^{\bullet} + H_2O$ | 4.50×10^8 | (McKenzie et al., 2016) |
| 48 $H^{\bullet} + NO_2^- \rightarrow NO^{\bullet} + OH^-$ | 7.10×10^8 | (McKenzie et al., 2016) |
| 49 $HNO_2 \rightarrow H^{\bullet} + NO_2^-$ | 3.00×10^7 | (McKenzie et al., 2016) |
| 50 $H^{\bullet} + NO_2^- \rightarrow HNO_2$ | 5.00×10^{10} | (McKenzie et al., 2016) |

The experimental data that were used for the calibration were performed in air environment. This means that this model can be used to calibrate and optimise the system. Regarding the totally different outcome of the fractions of the radicals in both models, there will be investigated if these fractions are rather correct or incorrect.

4.4 Extension of the model – reactions with pharmaceuticals

Once a good working and realistic model was obtained, a first extension was made introducing pharmaceuticals inside the system. Using available data from the University of Antioquia, two pharmaceuticals were selected. The pharmaceuticals CIP and ACE were selected. The degradation reaction of the pharmaceuticals only consists of the reactions with the hydroxyl radical as the hydrogen peroxide is too stable to interact. The reactions of both pharmaceuticals are showed below in Figure 23 and Figure 24.

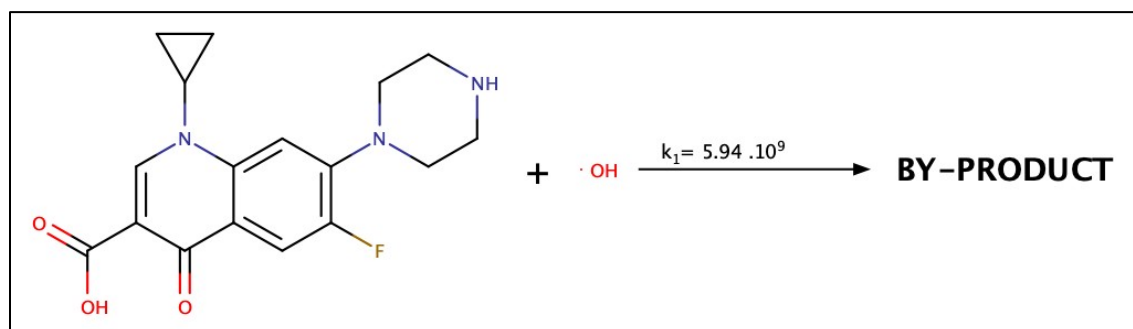


Figure 23: Ciprofloxacin reaction and reaction rate constant with hydroxyl radical

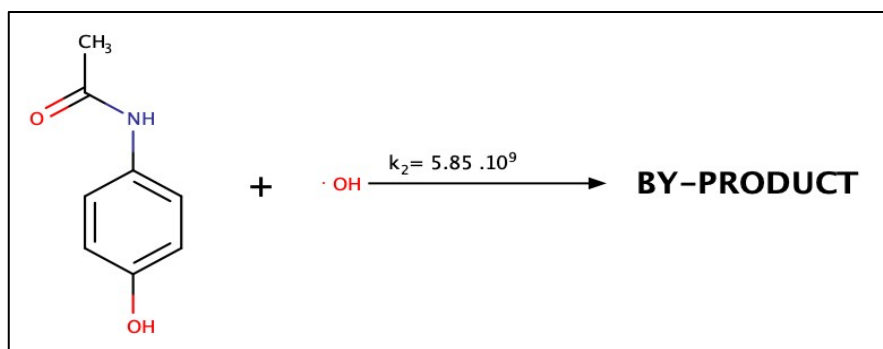


Figure 24: Acetaminophen reaction and reaction rate constant with hydroxyl radical

Both reactions are reacting producing several by-products. These by-products will be consumed as well. The precise rate constant of these by-products are not easy to determine neither it is easy to describe the interference of these by-products with the degradation reaction of the target components.

CHAPTER 5: RESULTS AND DISCUSSION

5.1 Introduction

In this chapter, the results of the models will be displayed and discussed. Both models will be described separately and will be compared with each other. The comparison will be made because of the big difference in the species fractions of the hydroxyl radical and the hydrogen peroxide.

The model based on Yasui will be discussed more in detail. This is due to the experimental data obtained from the experiments in the lab. These experiments include the concentration profile of hydrogen peroxide. There was tried to find similar results for the hydrogen peroxide profile by using different values for the magnitude of POWER.

To give a realistic example of the used codes an example of a used Root.eqn, Root.def, Root.spc and Root.kpp-file are added as appendix I, II, III and IV respectively.

5.2 Merouani model

The model based on the findings of Merouani (et al.) was used for simulations in oxygen saturated media. In the following figures, an example of the simulations for all the important radicals and species are presented. In Figure 25a continuous sonication of 20 minutes was used, in Figure 26 the impulse function was used (three cycles of 30 seconds on - 10 seconds off). Note that only short impulse times in terms of seconds-minutes were possible with the used numerical method. In both figures, the most important to follow radicals are displayed.

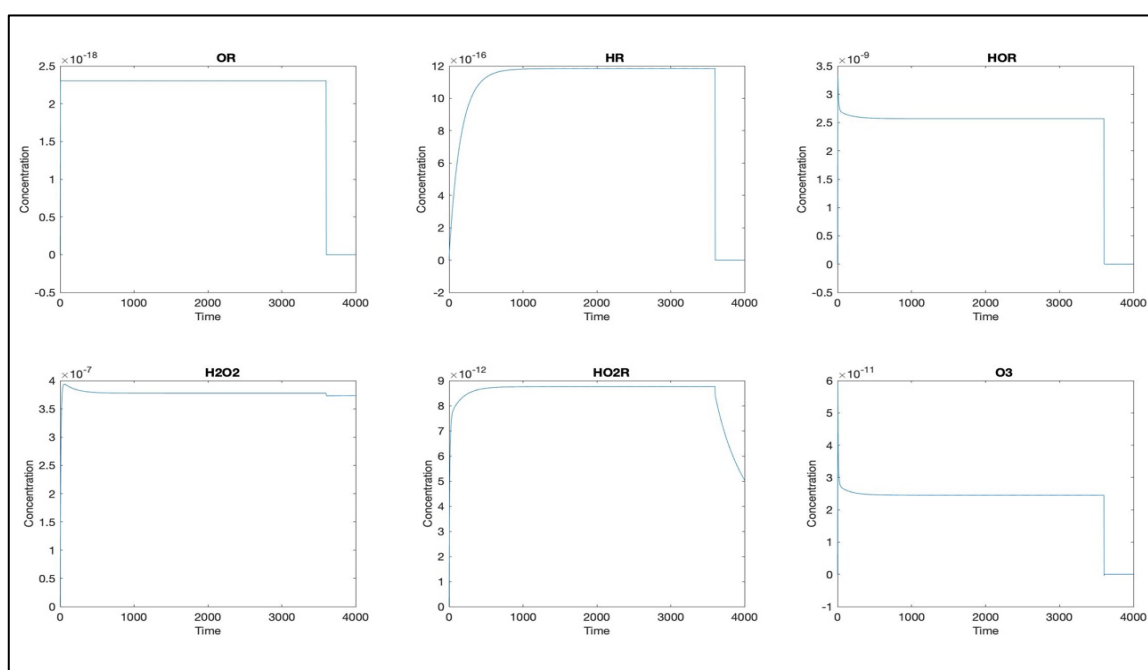


Figure 25: Simulation results in an oxygen atmosphere using 1 hour (3600 s) of sonication. Concentrations are in moles per litre (M) and time in seconds. The used value of POWER was $1.06E-7 \text{ M}\cdot\text{s}^{-1}$. The names of the common reactive species: OR is oxygen radical, HR is hydrogen radical, HOR is hydroxyl radical, H2O2 is hydrogen peroxide, HO2R is perhydroxyl radical and O3 is ozone. Plot created with Matlab

STUDY OF RADICAL CHEMISTRY IN ADVANCED OXIDATION PROCESSES BASED ON ULTRASOUND RADIATION IN WATER FOR PHARMACEUTICAL DRUGS REMOVAL

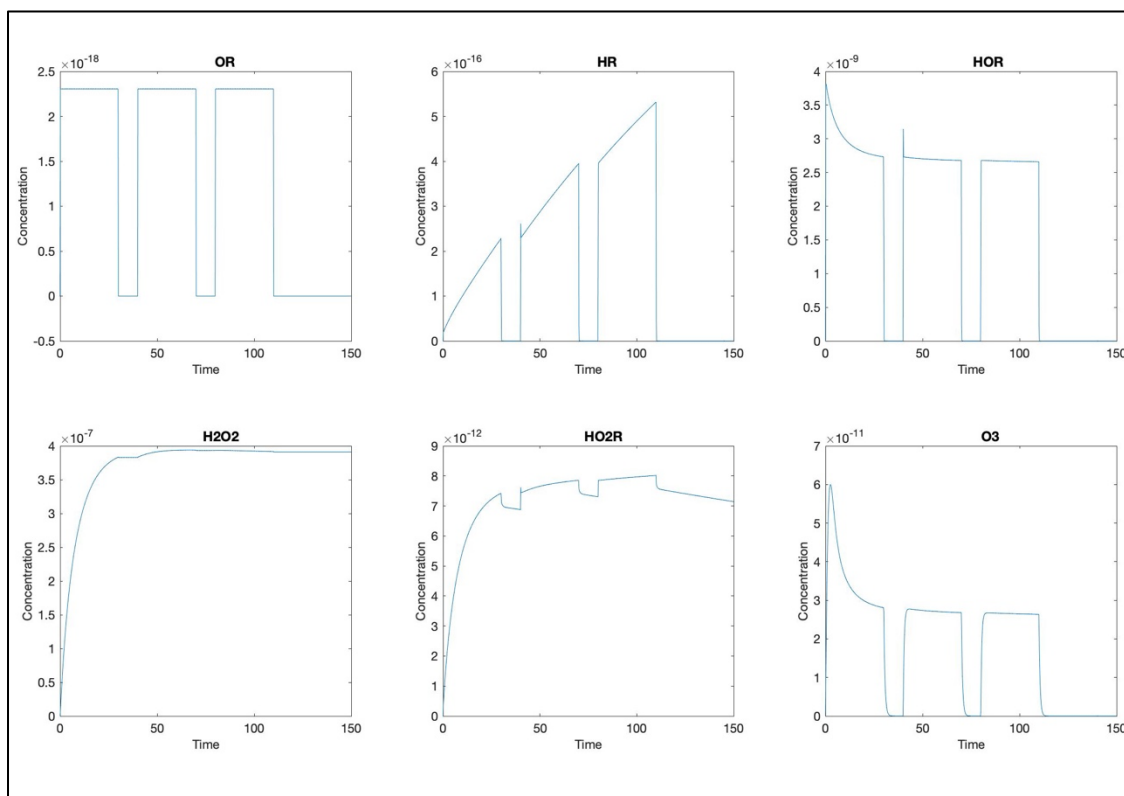


Figure 26: Simulation results in an oxygen atmosphere using impulse sonication of 30 seconds on-10 seconds off. Concentrations are in moles per litre (M) and time in seconds. The used value of POWER was $1.06E-7 \text{ M}\cdot\text{s}^{-1}$. The names of the common reactive species: OR is oxygen radical, HR is hydrogen radical, HOR is hydroxyl radical, H2O2 is hydrogen peroxide, HO2R is perhydroxyl radical and O3 is ozone. Plot created with Matlab

The impulse method can be useful for future research. Using an alternating on/off way of sonication can give similar results in terms of radical species generation but a lower energy consumption. The area underneath the hydroxyl radical peaks can be used to determine the best impulse times. The impulse method is not further used in this work and is just showed as an example of possible outputs when using continuous or alternating radiation.

Due to no experiments carried out in oxygen environment, the system was not calibrated in these circumstances yet. Besides that, this information can be used in the future to build further on the optimization of the system and model.

5.3 Yasui model

The model based on the findings of Yasui (et al.) was the most useful model because of the availability of experimental data. First, the model was calibrated in pure water environment and a sonication time of 20 minutes. Afterwards, the model was extended for longer sonication periods (2.5 hours) and sonication of water containing the pharmaceutical components ACE and CIP. In the following sections, each step of calibration is described and discussed.

5.3.1 Short sonication times

For the first calibration, short sonication times were evaluated. The aim here was to find a way to connect the simulations with the experimental findings only changing the value of POWER. The only reliable data is the concentration profile of hydrogen peroxide. During 20 minutes of sonication, four samples were taken, and the hydrogen peroxide concentration was calculated using iodometric techniques. The resulting profile was then calibrated. This was done by iteratively changing the value of POWER until similar profiles were obtained. Experiments were carried out using different acoustic powers. This made it possible to evaluate the correlation of the POWER value (in $M \cdot s^{-1}$) to the acoustic power density (in W/L). The power density was used to have a more uniform value for the acoustic power. The results of the calibration are showed in Figure 27. The dots are the experimentally found concentrations of hydrogen peroxide in time at different acoustic powers, the solid lines are the simulation curves for hydrogen peroxide.

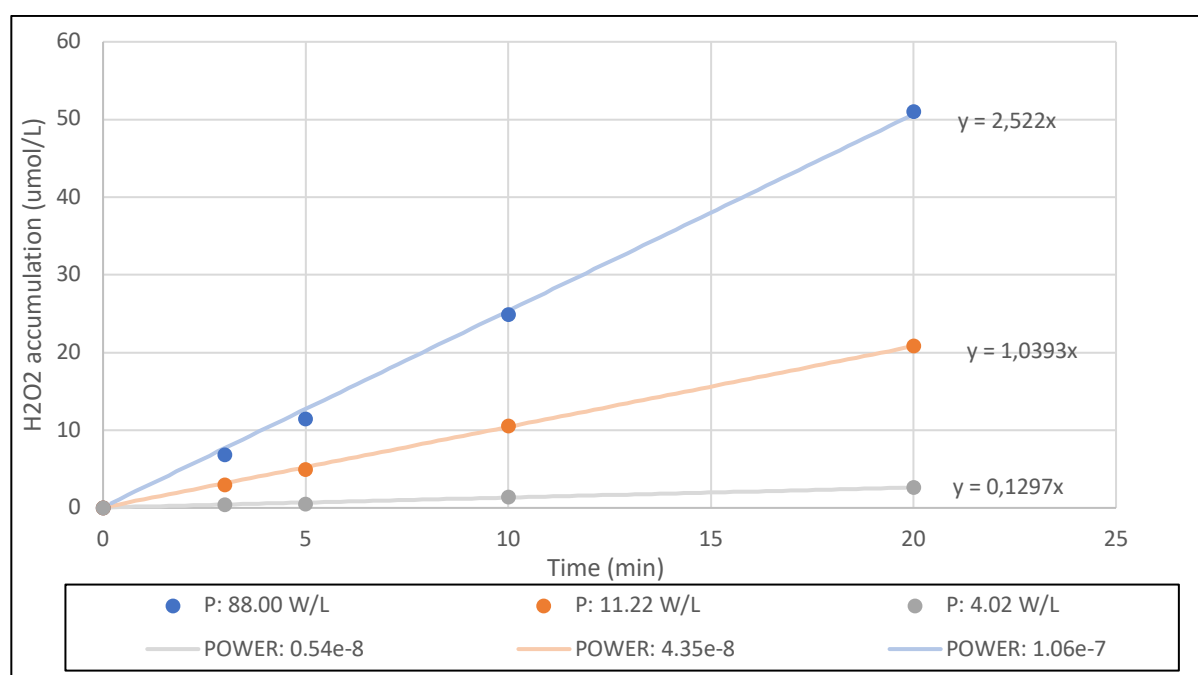


Figure 27: Calibration results for short sonication times (20 minutes). The dots are experimentally found, the lines represent the simulation data

In this first calibration, similar profiles were obtained. For each acoustic power irradiated to the water, a complementary value for POWER was found iteratively. Still, not enough data is available to be completely sure of the used values. In a further state of research, the magnitude of POWER can be divided into different sources like the frequency, acoustic amplitude and maybe other parameters as the mass transfer, physical properties of the media, etc..

5.3.2 Long sonication time (2.5 hours)

Due to promising results on shorter timeframes, experiments were done for longer period. The experiment was only done using 88.00 W/L of acoustic power (density), measuring the hydrogen peroxide concentration in time. The results are shown in Figure 28.

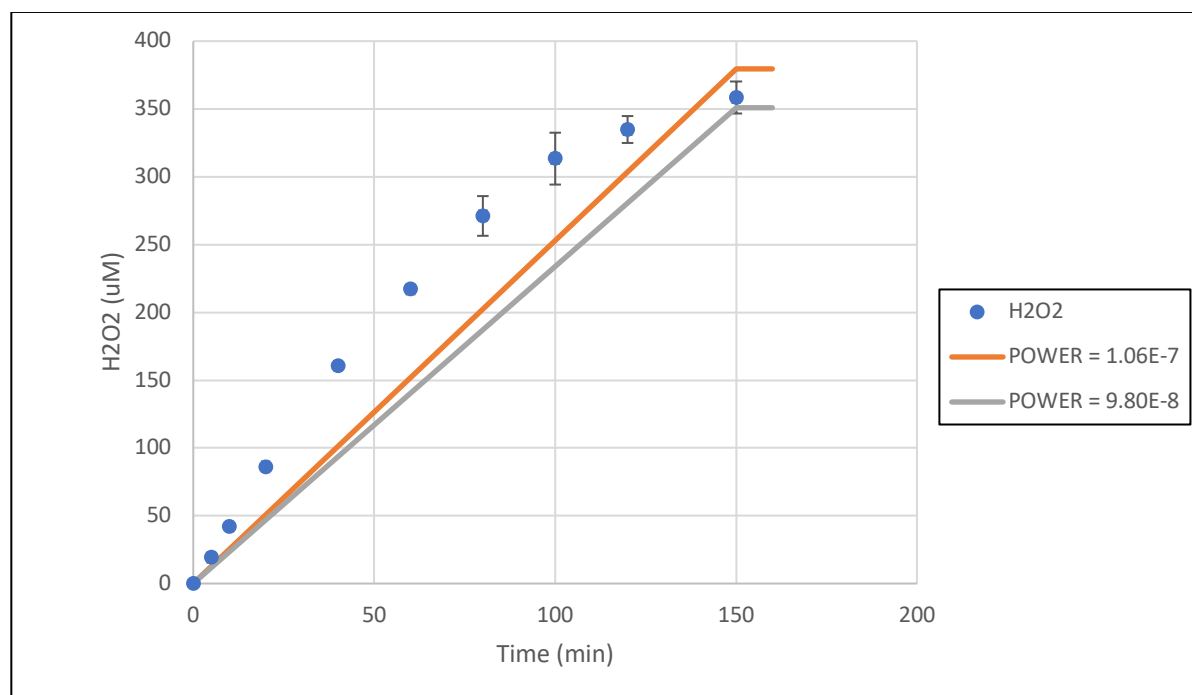


Figure 28: Calibration results of long sonication time (2.5 hours) using an acoustic power density of 88.00 W/L. The blue dots are the experimentally found concentrations, the lines are the profiles found by simulations

It is clear that, for longer sonication periods (longer than 20 minutes), the simulations show a different concentration profile. One of the reasons that could explain this is the source reaction. Looking back to the source reaction Φ , it is something that could be expected since the amount of hydroxyl radicals that is produced by the acoustic cavitation compared with the hydrogen peroxide production is very low. Due to the high fraction of hydrogen peroxide in the source function, a linear correlation is found in the simulations.

Regarding the fractions of $\cdot\text{OH}$ and H_2O_2 produced by acoustic cavitation, a big difference is noticeable. The comparison of both source reactions are showed in Table 10 (hydroxyl radical and hydrogen peroxide are indicated in bold). When looking to the model with oxygen, almost 70 % of all reactive species created are $\cdot\text{OH}$ compared to 2 % in air atmosphere. This gives an indication that more $\cdot\text{OH}$ is produced than predicted by Yasui or that the model is not complete. This model is a result of a study done with reactions and their reaction rate constants obtained from the theory. There is a possibility that other reactions or phenomena take place that is not yet discovered by researchers. Probably the difference in diffusivity can be one of the problems as the model does not include mass transfer phenomena.

Table 10: Comparison of production fractions of both models (oxygen and air atmosphere)

| Species | O ₂ (Merouani) | Air (Yasui) |
|-----------------------------------|---------------------------|--------------|
| NO [•] | / | 3.88E-05 |
| NO ₂ [•] | / | 0.0003 |
| H [•] | 0.0163 | 0.0004 |
| NO ₃ [•] | / | 0.0008 |
| N ₂ O | / | 0.002 |
| •OH | 0.6988 | 0.018 |
| H ₂ | 0.0489 | 0.021 |
| HNO ₃ | / | 0.031 |
| HNO ₂ | / | 0.078 |
| O ₃ | 0.00054 | 0.098 |
| O [•] | 0.2174 | 0.129 |
| HO ₂ [•] | 0.0163 | 0.129 |
| H₂O₂ | 0.0017 | 0.492 |

Because of the big difference in fraction of •OH, new simulations were run, changing the ratio of •OH/H₂O₂-fractions. Increasing the production of •OH can give an indication if Yasui's predictions are rather reliable or not. In Figure 29 the results of changing the •OH/H₂O₂-fractions ratio is showed. Analysing the concentration profiles, it is seen that when increasing the •OH fraction, results in a decrease of the slope. When increasing the ration above 1, a non-linear pattern is found in the beginning of the sonication. Notice when the •OH fraction becomes too high (the ratio above 1), The POWER value needs to be adjusted to have a noticeable change regarding the other simulations.

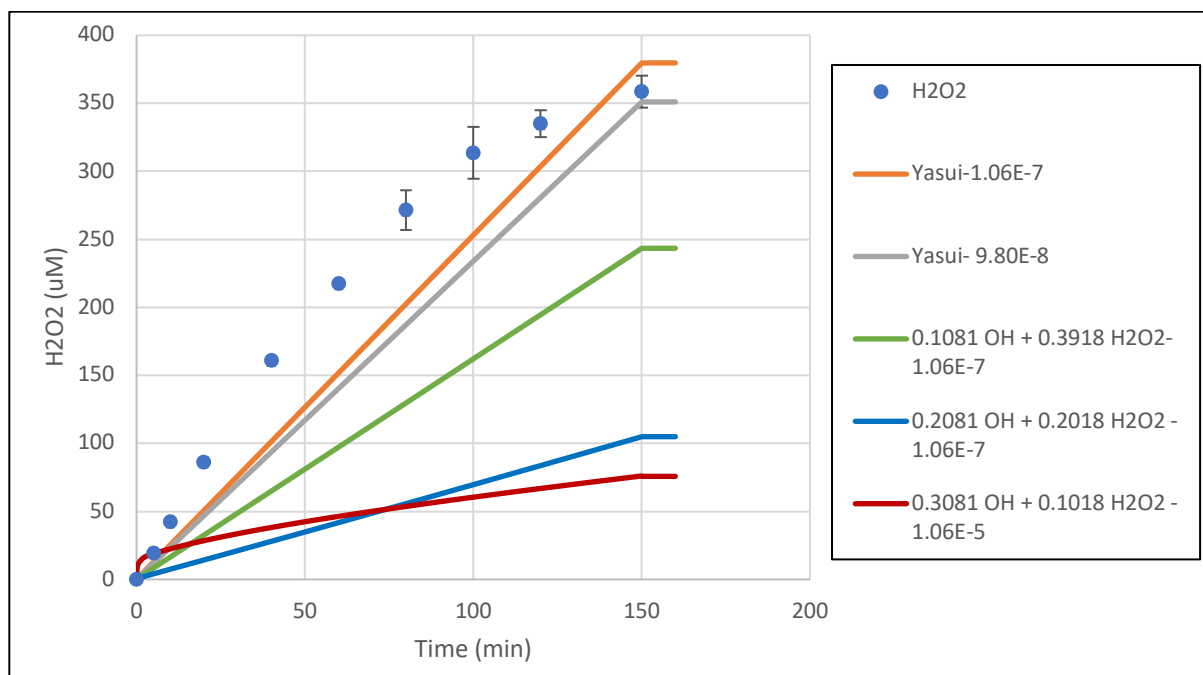


Figure 29: Calibration results of long period (2.5 h) changing the OH/H₂O₂ fraction ratio. The values in the legend are the fractions used in the simulations and the POWER value is presented after the "-". Dots are the experimentally found values, the lines are simulation.

Besides the hydrogen peroxide analysis, the pH was also followed in time. Since acid-base reactions are inside the model, a comparison of the pH pattern could be made. The resulting comparison is showed in Figure 30.

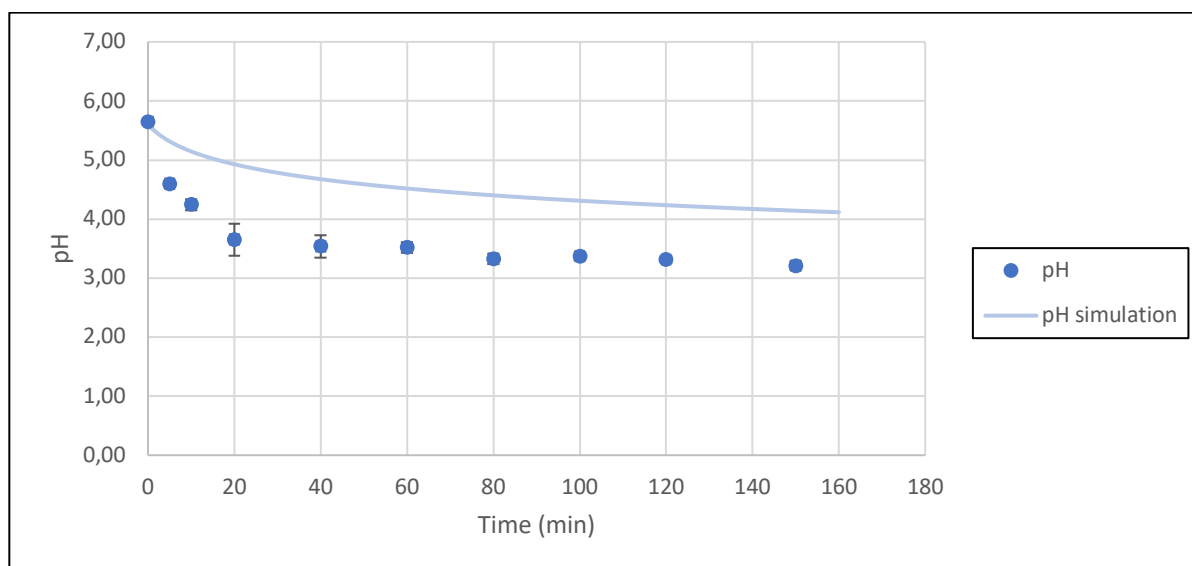


Figure 30: Comparison of the pH for long term experiments. The dots indicate the experimental data, the line is the profile found from simulation

In experiments and simulation, the pH decreases by time. Only, in the simulations the big increase in proton concentration is not in the same magnitude as experimentally found. This gives an indication that also in the model, something is missing. Besides that, the acid-base reaction rate constants are not always determined in the past due to the still unknown properties of the proton (H^+ or H_3O^+ ?).

Regarding all the data obtained and compared for longer periods than 20 minutes, it is clear that the model is most likely not complete or there are effects (as mass transfer) that are ignored in the model.

5.3.3 Sonication of water containing pharmaceuticals

Thirdly, some experiments were done with pharmaceuticals ACE and CIP. The data of two experiments were used for comparison with the simulations. The first experiment was the degradation of the pharmaceuticals ($C_{\text{pharmaceutical, initial}} = 3.3 \mu\text{M}$) for 30 minutes of sonication, the second experiment was measuring the production of H_2O_2 with and without presence of CIP. For these experiments, the model was updated using the reaction rate constant found in literature and simulations were done using $1.06\text{E-}7$ as the value for POWER. The combined results are shown in Figure 31.

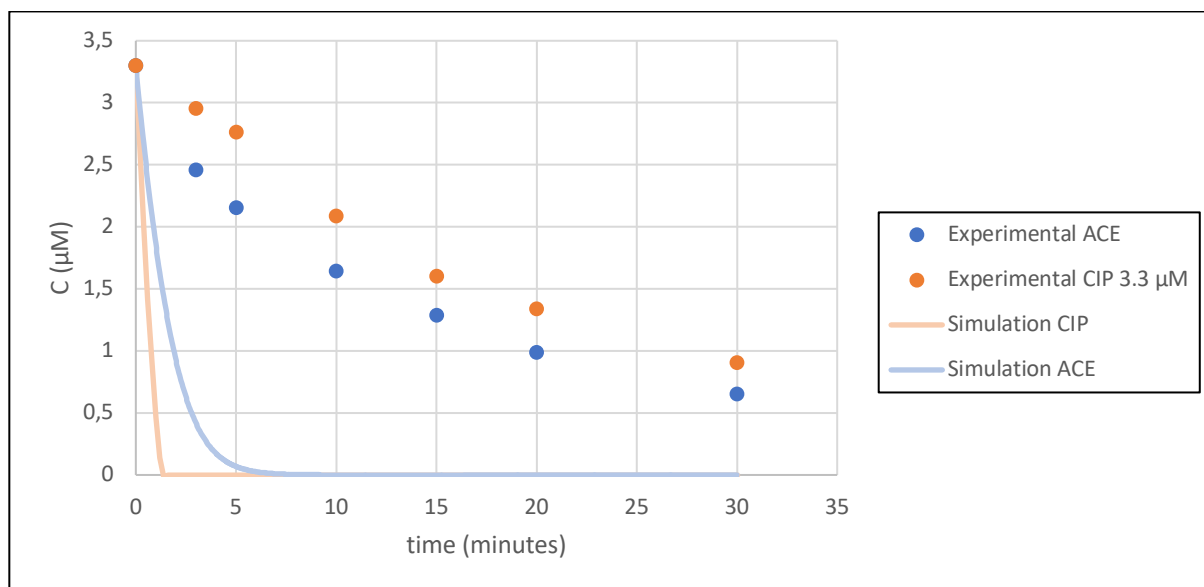


Figure 31: Combined results of the degradation of $3.31 \mu\text{M}$ pharmaceutical compounds. The dots are presenting the experimental data, the lines the simulation data. The simulations were done using $\text{POWER} = 1.06\text{E-}7 \text{ M}\cdot\text{s}^{-1}$

There is noticed that the degradation pattern is completely different for experimental and simulation data. This can be due to several things: The model is not complete, the mass transfer from the bubble wall to the molecules is not included in the model (which is true) or other unknown phenomena are slowing down the reaction of the pharmaceuticals with the hydroxyl radicals.

Another reason could be that the hydroxyl radicals are reacting with other components during time instead of reacting with the pharmaceuticals. This can be due to a competition that is created with the by-products of the pharmaceuticals. They can act as a scavenger for the hydroxyl radicals. Also, the mass transport from the bubble wall to the molecules can change during the sonication. A way to solve these phenomena in a first way is to insert a hydroxyl scavenger reaction like: **By-Product + $\cdot\text{OH}$ \rightarrow Products** with a faster reaction rate then the additional pharmaceutical reaction.

This latter idea was carried out using the original reaction rate constant for the scavenger reaction and reducing the reaction rate constant of the pharmaceutical (in this case CIP) a hundred times. The resulting simulations are showed in Figure 32. The simulations were only compared with a second experiment where the initial concentration of CIP was $40 \mu\text{M}$.

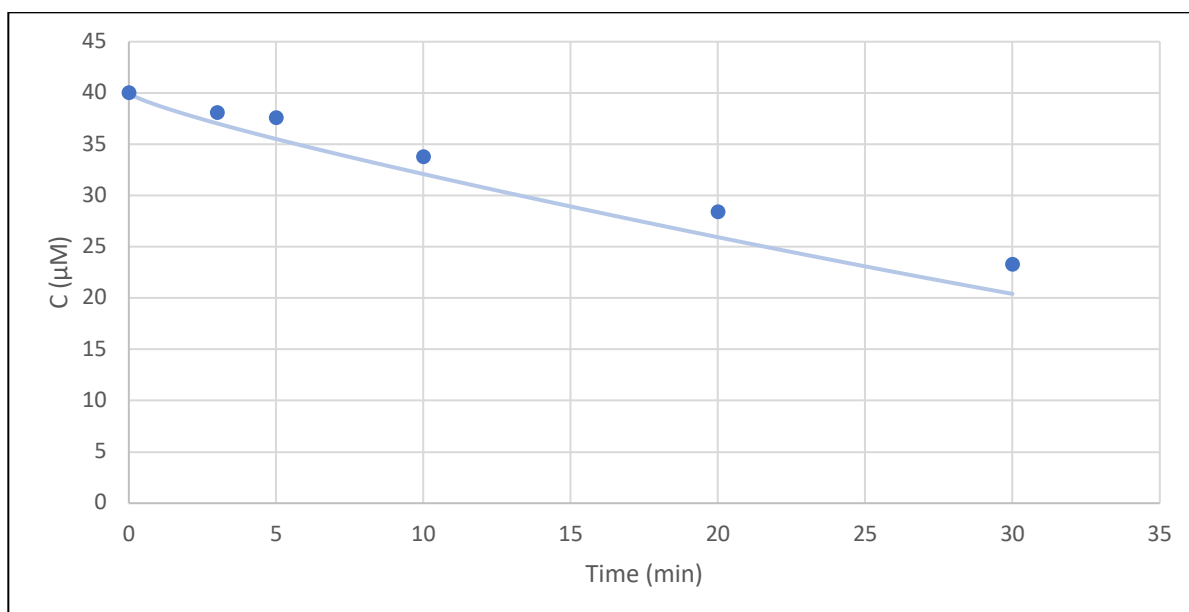


Figure 32: Degradation of 40 μM CIP, experimental results compared with simulations. The blue dots indicate the experimental results and the line the simulation results. Reaction rate constants were set as $k_{1,\text{CIP}} = 2.15\text{E}+8$ and $k_{2,\text{by-product}} = 2.15\text{E}+10$

This result can indicate that possible scavenger reactions are taking place, reducing the reactivity of the pharmaceutical itself. Au contraire, more experimental results are needed to justify this assumption.

During the degradation experiments, the concentration of hydrogen peroxide was also measured. In the experimental data, a decrease of hydrogen peroxide production was found when CIP was present in the solution. This information could be used to check if simulations found similar outcomes. The findings are presented in Figure 33.

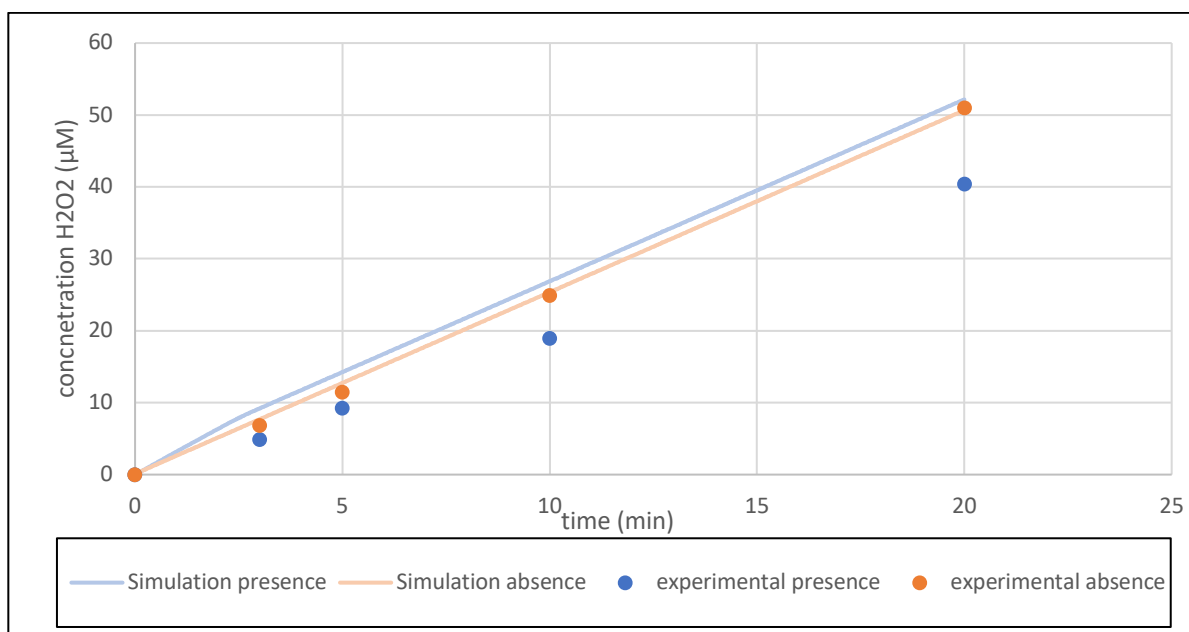


Figure 33: Comparison of the H_2O_2 concentration during sonication in presence and absence of CIP. Dots are presenting the experimental data and the lines the simulations.

It is seen that when CIP is presented in the solution, simulations give an even higher production of H_2O_2 instead of lower. Again, it indicates that something in the model is missing. The higher production of the hydrogen peroxide in the simulations can be due to the reaction of H_2O_2 and $\cdot OH$ that is cancelled out because of the reaction with the pharmaceutical. Because of that the H_2O_2 never get consumed and in that turn gives a higher increase. Again, more comparasions need to be made to confirm these interpretations.

CHAPTER 6: CONCLUSION

In this work, a first approach of a model for acoustic cavitation phenomena in the aqueous phase in pure water and water containing pharmaceuticals was introduced. This model includes aqueous radical and acid-base reactions that are most likely to occur regarding the literature. The reactions in the model were simulated using a chemical simulation program KPP.

The model was created by using two references (Merouani (et al.) and Yasui (et al.)). Using their data two models were created. One for oxygen saturated environment (based on Merouani) and one for air saturated environment (based on Yasui). For each model a source reaction was used that was related to the fractions of radical species that are created inside the cavitation bubbles. To change the concentration of radical species produced by the cavitation, a magnitude POWER ($M.s^{-1}$) was used. This magnitude is a general value for the reaction rate constant of the source term reaction. POWER includes now a variety of parameters as the acoustic power, the frequency of the US, the reactor parameters (as reaction volume, height, ...) and maybe more. It has to be split up in all the different variables that have influence on the production of the radicals in the future.

The model based on Yasui could be used for a first calibration using experimental data. Calibration was most of the time done by comparing the concentration of hydrogen peroxide (H_2O_2) in time. First, the model was calibrated for short sonication times (20 minutes) at different acoustic powers. The simulations were carried out by iteratively changing the POWER value until similar results compared to the experiments were found. This made it possible to set a first estimation of the value for POWER for further simulations. For the next acoustic power densities, the following value of POWER was determined: 4.02 W/L ($0.54 \cdot 10^{-8} M.s^{-1}$), 11.22 W/L ($4.35 \cdot 10^{-8} M.s^{-1}$) and 88.00 W/L ($1.06 \cdot 10^{-7} M.s^{-1}$).

Because of the promising first calibration, sonication for longer period (2.5 hours) was done. The calibration of longer periods showed that the concentration of H_2O_2 after 2.5 hours was similar, but the concentration profile was different. This was a first indication that probably something in the model needs to be optimised, if longer sonication periods (>30 minutes) are wished. There was tried to find a solution by changing the production of $\cdot OH$ and H_2O_2 by changing the fractions (increasing production of $\cdot OH$ and decreasing production of H_2O_2) in the source reaction. This led to a decrease in H_2O_2 in general, but no similar fit was found. In this experiment, pH measurements were done as well. Comparing this with the output of the simulation, a similar profile was found. Au contraire, the decrease of pH in the beginning of sonication was higher in experiments than in the simulations. This again gives an indication that the model is incomplete for the acid-base reactions.

Thirdly, a first model including pharmaceutical compounds was generated. The pharmaceuticals used were ciprofloxacin (CIP) and acetaminophen (ACE). The experiments were always with one component at the time, sonicating for 30 minutes. Again, using the model, a different outcome was seen. The decrease of the concentration of the pharmaceuticals was too fast regarding to the experimental data. This was probably due to mass transfer effects and the scavenging properties of the by-products produced by the reaction of $\cdot OH$ with the pharmaceuticals. Another approach was tried by introducing the scavenger reaction $\cdot OH + \text{By-product} \rightarrow \text{products}$ and decreasing the reaction rate of reaction $\cdot OH + \text{CIP} \rightarrow \text{By-product}$ a hundred times. This latter gave a similar outcome, but it is too early to tell if this method can be justified because there was only one experiment to compare with.

STUDY OF RADICAL CHEMISTRY IN ADVANCED OXIDATION PROCESSES BASED ON ULTRASOUND RADIATION IN WATER FOR PHARMACEUTICAL DRUGS REMOVAL

In general, the model can be used for short sonication periods (maximum 30 minutes) but first, the correlation of the value POWER must be calibrated in more circumstances (different frequencies and acoustic powers). For longer periods and pharmaceutical removal, more data is needed to calibrate the system and probably additional (maybe still unknown) reactions are missing in the model.

Still, this work can be an introduction for students or researchers to start working on the optimization of the model or to try another approach using the findings of this work.

STUDY OF RADICAL CHEMISTRY IN ADVANCED OXIDATION PROCESSES BASED ON ULTRASOUND RADIATION IN
WATER FOR PHARMACEUTICAL DRUGS REMOVAL

REFERENCES

- Ashokkumar, M., 2011. The characterization of acoustic cavitation bubbles – An overview. *Ultrason. Sonochem.* 18, 864–872. <https://doi.org/10.1016/j.ultsonch.2010.11.016>
- Barbusinski, K., 2009. FENTON REACTION - CONTROVERSY CONCERNING THE CHEMISTRY. *Cological Chem. Eng. S* 16, 347–358.
- Beltrán, F.J., 2004. Ozone reaction kinetics for water and wastewater systems. Lewis Publishers, Boca Raton, Fla.
- Bezbarua, B.K., Reckhow, D.A., 2004. Modification of the Standard Neutral Ozone Decomposition Model. *Ozone Sci. Eng.* 26, 345–357. <https://doi.org/10.1080/01919510490482179>
- Bhangu, S.K., Ashokkumar, M., 2016. Theory of Sonochemistry. *Top. Curr. Chem.* 374, 56. <https://doi.org/10.1007/s41061-016-0054-y>
- Braeutigam, P., 2016. Degradation of Organic Micropollutants by Hydrodynamic and/or Acoustic Cavitation, in: *Handbook of Ultrasonics and Sonochemistry*. Springer Singapore, Singapore, pp. 761–783. https://doi.org/10.1007/978-981-287-278-4_56
- Brotchie, A., Statham, T., Zhou, M., Dharmarathne, L., Grieser, F., Ashokkumar, M., 2010. Acoustic Bubble Sizes, Coalescence, and Sonochemical Activity in Aqueous Electrolyte Solutions Saturated with Different Gases. *Langmuir* 26, 12690–12695. <https://doi.org/10.1021/la1017104>
- Burkholder, J.B., Sander, S.P., Abbatt, J., Barker, J.R., 2019. JPL Publication 19-5. Chemical Kinetics and Photochemical Data for Use in Atmospheric Studies 1610. <http://jpldataeval.jpl.nasa.gov/>
- Buxton, G.V., Greenstock, C.L., Helman, W.P., Ross, A.B., 1988. Critical Review of rate constants for reactions of hydrated electrons, hydrogen atoms and hydroxyl radicals ($\cdot\text{OH}/\cdot\text{O}^-$ in Aqueous Solution. *J. Phys. Chem. Ref. Data* 17, 513–886. <https://doi.org/10.1063/1.555805>
- Camargo-Perea, A.L., Serna-Galvis, E.A., Lee, J., Torres-Palma, R.A., 2021. Understanding the effects of mineral water matrix on degradation of several pharmaceuticals by ultrasound: Influence of chemical structure and concentration of the pollutants. *Ultrason. Sonochem.* 73, 105500. <https://doi.org/10.1016/j.ultsonch.2021.105500>
- Chatel, G., Novikova, L., Petit, S., 2016. How efficiently combine sonochemistry and clay science? *Appl. Clay Sci.* 119, 193–201. <https://doi.org/10.1016/j.clay.2015.10.019>
- Ciawi, E., Rae, J., Ashokkumar, M., Grieser, F., 2006. Determination of Temperatures within Acoustically Generated Bubbles in Aqueous Solutions at Different Ultrasound Frequencies. *J. Phys. Chem. B* 110, 13656–13660. <https://doi.org/10.1021/jp061441t>
- Damian, V., Sandu, A., Damian, M., Potra, F., Carmichael, G.R., 2002. The kinetic preprocessor KPP-a software environment for solving chemical kinetics. *Comput. Chem. Eng.* 26, 1567–1579. [https://doi.org/10.1016/S0098-1354\(02\)00128-X](https://doi.org/10.1016/S0098-1354(02)00128-X)
- Dukane, 2010. How does your ultrasonic probe/stack work? [WWW Document]. URL <https://www.dukane.com/blog/2010/03/11/how-does-your-ultrasonic-probestack-work/> (accessed 4.10.21).
- Ershov, B.G., Gordeev, A.V., 2008. A model for radiolysis of water and aqueous solutions of H₂, H₂O₂ and O₂. *Radiat. Phys. Chem.* 77, 928–935. <https://doi.org/10.1016/j.radphyschem.2007.12.005>
- Gao, Y., Gao, N., Deng, Y., Gu, J., Gu, Y., Zhang, D., 2013. Factors affecting sonolytic degradation of sulfamethazine in water. *Ultrason. Sonochem.* 20, 1401–1407. <https://doi.org/10.1016/j.ultsonch.2013.04.007>
- Ge, C., 2015. Numerical Simulation of Vibration Deflection Effects on the Energy Efficiency of Ultrasonic Transducer for Sonochemistry. *Math. Probl. Eng.* 2015, 1–9. <https://doi.org/10.1155/2015/591352>

- Gielen, B., Marchal, S., Jordens, J., Thomassen, L.C.J., Braeken, L., Van Gerven, T., 2016. Influence of dissolved gases on sonochemistry and sonoluminescence in a flow reactor. *Ultrason. Sonochem.* 31, 463–472. <https://doi.org/10.1016/j.ultsonch.2016.02.001>
- Gogate, P.R., Patil, P.N., 2016. Sonochemical Reactors. *Top. Curr. Chem.* 374, 61. <https://doi.org/10.1007/s41061-016-0064-9>
- Gonzalez, M.C., Mártire, D.O., 1997. Kinetics of O and O in alkaline aqueous solutions. *Water Sci. Technol.* 35. [https://doi.org/10.1016/S0273-1223\(97\)00008-5](https://doi.org/10.1016/S0273-1223(97)00008-5)
- Gwadi, A., 2011. Application of advanced oxidation process for reducing the volume of an aeration tank of a conventional wastewater treatment plant 9, 60–69.
- Hairer, E., Wanner, G., 1996. Solving Ordinary Differential Equations II, Springer Series in Computational Mathematics. Springer Berlin Heidelberg, Berlin, Heidelberg. <https://doi.org/10.1007/978-3-642-05221-7>
- Haland, S.H., Gowri, G., Sowndhariyaa, M., Divyaparkavi, K., 2017. Hybrid Energy Generation from Acoustic and Pressure Waves using Piezoelectric Transducers. *International Journal for Modern Trends in Science and Technology*, 3, 178–182. <https://doi.org/10.13140/RG.2.2.33766.47686>
- Henglein, A., Kormann, C., 1985. Scavenging of OH Radicals Produced in the Sonolysis of Water. *Int. J. Radiat. Biol. Relat. Stud. Phys. Chem. Med.* 48, 251–258. <https://doi.org/10.1080/09553008514551241>
- Ince, N.H., Tezcanli, G., Belen, R.K., Apikyan, İ.G., 2001. Ultrasound as a catalyzer of aqueous reaction systems: the state of the art and environmental applications. *Appl. Catal. B Environ.* 29, 167–176. [https://doi.org/10.1016/S0926-3373\(00\)00224-1](https://doi.org/10.1016/S0926-3373(00)00224-1)
- Ingole, D.N.W., Khedkar, S.V., 2012. Review Article THE ULTRASOUND REACTOR TECHNOLOGY-A TECHNOLOGY FOR FUTURE. *Int. J. Adv. Eng. Res. Stud.* 2, 72–75.
- Kanakaraju, D., Glass, B.D., Oelgemöller, M., 2018. Advanced oxidation process-mediated removal of pharmaceuticals from water: A review. *J. Environ. Manage.* 219, 189–207. <https://doi.org/10.1016/j.jenvman.2018.04.103>
- Liu, J.-L., Wong, M.-H., 2013. Pharmaceuticals and personal care products (PPCPs): A review on environmental contamination in China. *Environ. Int.* 59, 208–224. <https://doi.org/10.1016/j.envint.2013.06.012>
- Mack, J., Bolton, J.R., 1999. Photochemistry of nitrite and nitrate in aqueous solution: a review. *J. Photochem. Photobiol. Chem.* 128, 1–13. [https://doi.org/10.1016/S1010-6030\(99\)00155-0](https://doi.org/10.1016/S1010-6030(99)00155-0)
- Mahamuni, N.N., Adewuyi, Y.G., 2010. Advanced oxidation processes (AOPs) involving ultrasound for waste water treatment: A review with emphasis on cost estimation. *Ultrason. Sonochem.* 17, 990–1003. <https://doi.org/10.1016/j.ultsonch.2009.09.005>
- McKenzie, H., MacDonald-Taylor, J., McLachlan, F., Orr, R., Woodhead, D., 2016. Modelling of Nitric and Nitrous Acid Chemistry for Solvent Extraction Purposes. *Procedia Chem.* 21, 481–486. <https://doi.org/10.1016/j.proche.2016.10.067>
- Mehrvar, M., Anderson, W.A., Moo-Young, M., 2001. Photocatalytic degradation of aqueous organic solvents in the presence of hydroxyl radical scavengers. *Int. J. Photoenergy* 3, 187–191. <https://doi.org/10.1155/S1110662X01000241>
- Merouani, S., Ferkous, H., Hamdaoui, O., Rezgüi, Y., Guemini, M., 2015a. A method for predicting the number of active bubbles in sonochemical reactors. *Ultrason. Sonochem.* 8.
- Merouani, S., Hamdaoui, O., Rezgüi, Y., Guemini, M., 2015b. Computer simulation of chemical reactions occurring in collapsing acoustical bubble: dependence of free radicals production on operational conditions. *Res. Chem. Intermed.* 41, 881–897. <https://doi.org/10.1007/s11164-013-1240-y>
- Merouani, S., Hamdaoui, O., Rezgüi, Y., Guemini, M., 2015c. Sensitivity of free radicals production in acoustically driven bubble to the ultrasonic frequency and nature of dissolved gases. *Ultrason. Sonochem.* 22, 41–50. <https://doi.org/10.1016/j.ultsonch.2014.07.011>

- Merouani, S., Hamdaoui, O., Rezgui, Y., Guemini, M., 2013. Effects of ultrasound frequency and acoustic amplitude on the size of sonochemically active bubbles – Theoretical study. *Ultrason. Sonochem.* 20, 815–819. <https://doi.org/10.1016/j.ultsonch.2012.10.015>
- Merouani, S., Oualid, H., Yacine, R., Miloud Guemini, 2014. Theoretical estimation of the temperature and pressure within collapsing acoustical bubbles. *Ultrason. Sonochem.* 21, 53–59.
- Mizuno, T., Tsuno, H., Yamada, H., 2007. Development of Ozone Self-Decomposition Model for Engineering Design. *Ozone Sci. Eng.* 29, 55–63. <https://doi.org/10.1080/01919510601115849>
- Moholkar, V.S., 2016. Mathematical Models for Sonochemical Effects Induced by Hydrodynamic Cavitation, in: *Handbook of Ultrasonics and Sonochemistry*. Springer Singapore, Singapore, pp. 625–671. https://doi.org/10.1007/978-981-287-278-4_51
- Mousally, S.M.M., Al-Zaydi, K.M., Petrier, C., Arab, S.T., Refat, M.S., 2019. Study of Sonochemical Effect on Dibenzothiophene in Deionized Water, Natural Water and Sea Water. *Sci. Adv. Mater.* 11, 1684–1691. <https://doi.org/10.1166/sam.2019.3612>
- mrcophth.com, n.d. The Principles of Medical Ultrasound [WWW Document]. URL <http://www.mrcophth.com/commonultrasoundcases/principlesofultrasound.html> (accessed 4.21.21).
- Naidu, D.V.P., Rajan, R., Kumar, R., Gandhi, K.S., Arakeri, V.H., Chandrasekaran, S., 1994. Modelling of a batch sonochemical reactor. *Chem. Eng. Sci.* 49, 877–888. [https://doi.org/10.1016/0009-2509\(94\)80024-3](https://doi.org/10.1016/0009-2509(94)80024-3)
- Neta, P., Huie, R.E., Ross, A.B., 1988. Rate Constants for Reactions of Inorganic Radicals in Aqueous Solution. *J. Phys. Chem. Ref. Data* 17, 1027–1284. <https://doi.org/10.1063/1.555808>
- Okitsu, K., Nanzai, B., Thangavadivel, K., 2016. Sonochemical Degradation of Aromatic Compounds, Surfactants, and Dyes in Aqueous Solutions, in: *Handbook of Ultrasonics and Sonochemistry*. Springer Singapore, Singapore, pp. 785–812. https://doi.org/10.1007/978-981-287-278-4_57
- piezodisk.com, 2018. Wat is piëzo-elektrische keramische materialen [WWW Document]. URL <http://m.nl.piezodisc.com/news/what-is-piezoelectric-ceramic-materials-14392314.html> (accessed 4.21.21).
- Ren, B., Shi, X., Jin, X., Wang, X.C., Jin, P., 2021. Comprehensive evaluation of pharmaceuticals and personal care products (PPCPs) in urban sewers: Degradation, intermediate products and environmental risk. *Chem. Eng. J.* 404, 127024. <https://doi.org/10.1016/j.cej.2020.127024>
- Ross, F., Ross, A.B., 1977. Selected specific rates of reactions of transients from water in aqueous solution. :: III. hydroxyl radical and perhydroxyl radical and their radical ions (No. NBS NSRDS 59). National Bureau of Standards, Gaithersburg, MD. <https://doi.org/10.6028/NBS.NSRDS.59>
- Sammuto Bartolo, N., Azzopardi, L.M., Serracino-Inglott, A., 2020. Pharmaceuticals and the environment. *Early Hum. Dev.* 3. <https://doi.org/10.1016/j.earlhumdev.2020.105218>
- Son, Y., 2016a. Advanced Oxidation Processes Using Ultrasound Technology for Water and Wastewater Treatment, in: *Handbook of Ultrasonics and Sonochemistry*. Springer Singapore, Singapore, pp. 711–732. https://doi.org/10.1007/978-981-287-278-4_53
- Son, Y., 2016b. Advanced Oxidation Processes Using Ultrasound Technology for Water and Wastewater Treatment, in: *Handbook of Ultrasonics and Sonochemistry*. Springer Singapore, Singapore, pp. 711–732. https://doi.org/10.1007/978-981-287-278-4_53
- Subedi, M.M., 2013. Ceramics and its Importance. *Himal. Phys.* 4, 80–82. <https://doi.org/10.3126/hj.v4i0.9433>
- Tiong, T.J., Liew, D.K.L., Gondipon, R.C., Wong, R.W., Loo, Y.L., Lok, M.S.T., Manickam, S., 2017. Identification of active sonochemical zones in a triple frequency ultrasonic reactor via physical and chemical characterization techniques. *Ultrason. Sonochem.* 35, 569–576. <https://doi.org/10.1016/j.ultsonch.2016.04.029>

- Tom Nelligan, n.d. An Introduction to Ultrasonic Transducers for Nondestructive Testing [WWW Document]. Olympus. URL <https://www.olympus-ims.com/en/resources/white-papers/intro-ultrasonic-transducers-ndt-testing/> (accessed 4.21.21).
- Torres-Palma, R.A., Serna-Galvis, E.A., 2018. Sonolysis, in: *Advanced Oxidation Processes for Waste Water Treatment*. Elsevier, pp. 177–213. <https://doi.org/10.1016/B978-0-12-810499-6.00007-3>
- Varga, R., Paál, G., 2015. Numerical investigation of the strength of collapse of a harmonically excited bubble. *Chaos Solitons Fractals* 76, 56–71. <https://doi.org/10.1016/j.chaos.2015.03.007>
- Yasui, K., 2018. *Acoustic Cavitation and Bubble Dynamics*, SpringerBriefs in Molecular Science. Springer International Publishing, Cham. <https://doi.org/10.1007/978-3-319-68237-2>
- Yasui, K., 2016. Unsolved Problems in Acoustic Cavitation, in: *Handbook of Ultrasonics and Sonochemistry*. Springer Singapore, Singapore, pp. 259–292. https://doi.org/10.1007/978-981-287-278-4_1
- Yasui, K., 2001. Effect of liquid temperature on sonoluminescence. *Phys. Rev. E* 64, 016310. <https://doi.org/10.1103/PhysRevE.64.016310>
- Yasui, K., Tuziuti, T., Iida, Y., 2004. Optimum bubble temperature for the sonochemical production of oxidants. *Ultrasonics* 42, 579–584. <https://doi.org/10.1016/j.ultras.2003.12.005>
- Yasui, K., Tuziuti, T., Kozuka, T., Towata, A., Iida, Y., 2007. Relationship between the bubble temperature and main oxidant created inside an air bubble under ultrasound. *J. Chem. Phys.* 127, 154502. <https://doi.org/10.1063/1.2790420>
- Yasui, K., Tuziuti, T., Lee, J., Kozuka, T., Towata, A., Iida, Y., 2008. The range of ambient radius for an active bubble in sonoluminescence and sonochemical reactions. *J. Chem. Phys.* 128, 184705. <https://doi.org/10.1063/1.2919119>

STUDY OF RADICAL CHEMISTRY IN ADVANCED OXIDATION PROCESSES BASED ON ULTRASOUND RADIATION IN WATER FOR PHARMACEUTICAL DRUGS REMOVAL

APPENDIX I: EXAMPLE EQUATION FILE

#EQUATIONS

// Hydroxyle and Hydroperoxide radical reactions

```
{1}  HOR + H2O2 = HO2R + H2O : 2.70E+7 ; // Ross
{2}  HOR + HO2N = O2RN + H2O : 7.50E+9 ; // JPL
{3}  ORN + H2O2 = O2RN + H2O : 5.00E+8 ; // Buxton
{4}  ORN + HO2N = O2RN + OH : 4.00E+8 ; // Buxton

{5}  HOR + HOR = H2O2 : 4.00E+9 ; // Ross
{6}  HOR + ORN = HO2N : 2.00E+10 ; // Buxton
//  ORN + ORN = HO2N + OH // Non reported reaction

{7}  HOR + HO2R = O2 + H2O : 1.00E+10 ; // JPL
{8}  HOR + O2RN = O2 + OH : 1.01E+10 ; // JPL
//  ORN + HO2R = O2 + OH // Non reported reaction
{9}  ORN + O2RN = O2 + 2 OH : 6.00E+8 ;

{10} ORN + O2 = O3RN : 3.60E+9 ; // Buxton
{11} ORN {+ H2O} = HOR + OH : 1.70E+6 ; // Buxton
{12} HOR + OH = H2O + ORN : 1.30E+10 ; // Buxton

{13} HO2R + HO2R = O2 + H2O2 : 3.40E+6 ; // Ross
{14} HO2R + O2RN = O2 + HO2N : 1.00E+8 ; // Ross
//  O2RN + O2RN = O2 + 2 OH // Non reported reaction

{15} HO2R + H2O2 = O2 + OH + H2O : 0.5 ; // Ross
{16} O2RN + H2O2 = O2 + OH + HOR : 0.13 ; // JPL
```

// Acid-Base Reactions

```
{17} HO2R = H + O2RN : 7.00E+5 ; // Ershov
{18} O2RN + H = HO2R : 4.50E+10 ; // Ershov

{19} H2O2 = H + HO2N : 3.56E-2 ; // Ershov
{20} HO2N + H = H2O2 : 2.00E+10 ; // Ershov

{21} H2O = H + OH : 2.50E-5 ; // Ershov
{22} H + OH = H2O : 1.40E+11 ; // Ershov
```

// Ozone Compounds

```
{23} O3 + OH = HO2R + O2 : 48 ; // Neta et al.
{24} O3 + OH = HO2N + O2RN : 70 ; // Neta et al.
{25} O3 + O2RN = O3RN + O2 : 1.52E+9 ; // Gonzalez
{26} O3 + HOR = HO2R + O2 : 1.10E+8 ; // Buxton
{27} O3 + H2O2 = HO3R + HO2R : 0.065 ; // Mizuno
```

STUDY OF RADICAL CHEMISTRY IN ADVANCED OXIDATION PROCESSES BASED ON ULTRASOUND RADIATION IN WATER FOR PHARMACEUTICAL DRUGS REMOVAL

{28} O3 + HO2N = O3RN + HO2R : 2.60E+6 ; // Bezbarua
 {29} HO3R = HOR + O2 : 1.10E+5 ; // Beltran
 {30} O3RN = ORN + O2 : 7.00E+8 ; // Ross
 {31} O3RN + HOR = HO2R + O2RN : 8.50E+9 ; // Buxton
 {32} O3RN + ORN = 2 O2RN : 7.00E+8 ; // Buxton

// Hydrogen Radical

{33} HR + O2 = HO2R : 2.10E+10 ; // JPL
 {34} HR + HO2R = H2O2 : 1.50E+10 ; // Buxton
 {35} HR + O2RN = HO2N : 2.00E+10 ; // Buxton
 {36} HR + H2O2 = HOR + H2O : 9.00E+7 ; // Buxton
 {37} HR + HOR = H2O : 7.00E+9 ; // Buxton
 {38} HR + HR = H2 : 1.55E+10 ; // Buxton
 {39} HR {+H2O} = HOR + H2 : 9.00E+7 ; // Buxton

// Oxygen Radical

{40} OR {+ H2O} = 2 HOR : 1.00E+10 ; // JPL

// No other reactions of OR are expected in water; HOR, HO2R, H2O2 are in low concentrations

// Nitrogen Compounds

{41} NOR + HOR = HNO2 : 1.00E+10 ; // Mack and bolton
 {42} NO2N + HOR = NO2R + OH : 1.00E+10 ; // Mack and bolton
 {43} NO2R + NOR = N2O3 : 1.10E+9 ; // Mack and bolton
 {44} N2O3 {H2O} = 2 HNO2 : 5.30E+2 ; // Mack and bolton
 {45} NO2R + NO2R = N2O4 : 4.50E+8 ; // Mack and bolton
 {46} N2O4 {H2O} = NO2N + 2 H + NO3N : 1.00E+3 ; // Mack and Bolton
 {47} HR + HNO2 = NO + H2O : 4.50E+8 ; // McKenzie
 {48} HR + NO2N = NO + OH : 7.10E+8 ; // McKenzie

// Acid-Base Reactions

{49} HNO2 = H + NO2N : 3.00E+7 ; // McKenzie
 {50} H + NO2N = HNO2 : 5.00E+10 ; // McKenzie

// Gases O2 + N2 + H2 (?)

{51} H2 + HOR = HR + H2O : 4.00E+7 ; // NSRDS-NBS-59
 {52} H2 + ORN = HR + OH : 8.00E+7 ; // Buxton
 {53} O3 + HR = HOR + O2 : 3.80E+10 ; // Neta et al.

// ULTRASOUND SOURCE GENERATION - Yasui

{61} US = 0.0004 HR : SonoSource() ;

STUDY OF RADICAL CHEMISTRY IN ADVANCED OXIDATION PROCESSES BASED ON ULTRASOUND RADIATION IN
WATER FOR PHARMACEUTICAL DRUGS REMOVAL

| | | | | |
|------|----|---|-------------|------------------|
| {62} | US | = | 0.0181 HOR | : SonoSource() ; |
| {63} | US | = | 0.1294 OR | : SonoSource() ; |
| {64} | US | = | 0.0207 H2 | : SonoSource() ; |
| {65} | US | = | 0.1294 HO2R | : SonoSource() ; |
| {66} | US | = | 0.4918 H2O2 | : SonoSource() ; |
| {67} | US | = | 0.0984 O3 | : SonoSource() ; |
| {68} | US | = | 0.0776 HNO2 | : SonoSource() ; |
| {69} | US | = | 0.0311 HNO3 | : SonoSource() ; |
| {70} | US | = | 0.0008 NO3R | : SonoSource() ; |
| {71} | US | = | 0.0003 NO2R | : SonoSource() ; |
| {72} | US | = | 0.00004 NOR | : SonoSource() ; |
| {73} | US | = | 0.0021 N2O | : SonoSource() ; |

APPENDIX II: EXAMPLE DEFINITION FILE

```
#include aquRadair.spc
#include aquRadair.eqn

#MONITOR      H; OH; HOR; H2O2; O3; OR; O2; HO2R;
#LOOKATALL

#INITVALUES

CFACTOR      = 1      ; {conversion}
ALL_SPEC     = 0.0    ;
O2           = 2.78E-4 ;
H2O         = 55.56  ;
H           = 1.0E-7;
OH          = 1.0E-7;
US         = 1.0    ;
N2         = 8.33E-4;

#INLINE MATLAB_GLOBAL
global RCNTRL ICNTRL POWER
#ENDINLINE

#INLINE MATLAB_INIT
global TSTART TEND DT TEMP RTOLS ATOLS RCNTRL ICNTRL POWER TAU DELTA CN
TSTART = 0.0;
RCNTRL = [0 1e-10 0 0.2 6 0.1 0.9];
ICNTRL = [1 0 0 0];
TEND = 1200;
DT = 1e-10;
TEMP = 298.15;
RTOLS = 1.0E-13;
ATOLS = 1.0E-13;
POWER = 1.06e-7;
TAU = 3600;
DELTA = 1000;
CN = 1;

#ENDINLINE
```

STUDY OF RADICAL CHEMISTRY IN ADVANCED OXIDATION PROCESSES BASED ON ULTRASOUND RADIATION IN
WATER FOR PHARMACEUTICAL DRUGS REMOVAL

```
#INLINE MATLAB_RATES
```

```
function [rate]=SonoSource()  
    global TIME POWER TAU DELTA CN;  
    rate=POWER*impulsetrain(TIME,TAU,DELTA ,CN);  
return
```

```
function y=impulsetrain(t,tau,delta,nc)  
    period=tau+delta;  
    ncy=floor(t/period);  
    tp=(t-ncy*period).*(ncy<nc)+(tau+delta/2).*(ncy>=nc);  
    y=heaviside(tp)-heaviside(tp-tau);  
return
```

```
#ENDINLINE
```

```
#INLINE C_INIT  
TSTART = 0.0;  
TEND = 120.0;  
DT = 0.05;  
TEMP = 298.15;  
#ENDINLINE
```

APPENDIX III: EXAMPLE SPECIES FILE

#include atoms

#DEFFIX

H2O = 2 H + O ;{water}
//O2 = O + O ;{oxygen, gas}
US = IGNORE ;{dummy, US power}
N2 = N + N ;{nitrogen, gas}
//N2O = 2 N + O ;{nitrous oxide, inert}

#DEFRAD

HOR = O + H ;{Hydroxyle radical}
ORN = O ;{Hydroxyle radical anion}
HO2R = O + O + H ;{Hydroperoxide radical}
O2RN = O + O ;{Hydroperoxide radical anion}
HO3R = 3 O + H ;{Hydroozonide radical}
O3RN = 3 O ;{Hydroozonide radical anion}
HR = H ;{Hydrogen radical}
OR = O ;{Oxygen radical}
NOR = N + O ;{Nitrogen oxide radical}
NO2R = 2 O + N ;{Nitrogen dioxide radical}
NO3R = 3 O + N ;{Nitrogen trioxide radical}
N2O = 2 N + O ;{nitrous oxide, inert}

#DEFVAR

H2O2 = 2 H + 2 O ;{Hydrogen peroxide}
HO2N = 2 O + H ;{Hydrogen peroxide anion}
OH = O + H ;{Hydroxide anion}
H = H ;{Proton cation}
O3 = 3 O ;{Ozone}
N2O3 = 2 N + 3 O ;{Dinitrogen trioxide}
N2O4 = 2 N + 4 O ;{Dinitrogen tetroxide}
HNO2 = H + N + 2 O ;{Nitrite Acid}
NO2N = N + 2 O ;{Nitrite anion}
HNO3 = H + N + 3 O ;{Nitric Acid}
NO3N = N + 3 O ;{Nitrate anion}
H2 = 2 H ;{Hydrogen}
NO = N + O ;{Nitrogen oxide}
O2 = O + O ;{oxygen, gas}

APPENDIX IV: EXAMPLE KPP FILE

```
#MODEL      aquRadair
#INTEGRATOR none
#INTFILE    Rosenbrock
#LANGUAGE   Matlab
#DRIVER     rosendrv
#JACOBIAN   SPARSE_LU_ROW
#HESSIAN    on
```

The end.

BUDGET COVER

Table of Contents

| | |
|-------------------------------------|---|
| 1. INTRODUCTION | 2 |
| 2. WORKFORCE CALCULATIONS | 2 |
| 3. MACHINE FORCE CALCULATIONS | 3 |
| 4. SUBCONTRACTORS | 4 |
| 5. TOTAL COST | 5 |
| 6. REFERENCES | 5 |

1. Introduction

In this chapter, a budget cover for this particular project will be described. The project was focused on developing a first theoretical chemical model for ultrasound radiation in water. For this, most of the work was done from home or office at the UPV. To have a good estimation of the costs of the project, machine and personnel costs are needed. Also, experimental data was used from the University of Antioquia Colombia and an estimation of this cost will be made as well. Due to the pandemic and the lack of specific laboratory equipment, no laboratory work was done by the student self.

For the realisation of this budget cover, the paper *Recomendaciones en la Elaboración de Presupuestos en Actividades de I+D+I (Revised version 2018)* from UPV was used.

The cost classification codes are shown in Table 1.

Table 1: Code classification for budget cover

| Code | Classification |
|------|----------------|
| WF | Workforce |
| MF | Machine force |
| MC | Material cost |

2. Workforce calculations

This work was carried out by the student, who will graduate as a chemical engineer, in collaboration with a tutor/professor of the nuclear and chemical department of UPV. In Table 2: Cost estimation of workforce all the workforce costs are listed. The worktime is an estimated worktime for student and tutor for creating the model, analysing the results, writing and reviewing the TFM.

Table 2: Cost estimation of workforce

| Code | Description | Price | | |
|-----------------------------|----------------------------------------|-------------------|--------------|------------------|
| | | Hourly cost (€/h) | Quantity (h) | Cost (€) |
| WF 1 | Graduate in Chemical engineering | 15.00 | 500 | 7500.00 |
| WF 2 | Project responsible (UPV tutor-expert) | 39.00 | 120 | 4680.00 |
| WF 3 | Subcontractor – PhD technical | 23.80 | 15 | 357.00 |
| TOTAL WORKFORCE COST | | | | 12 537.00 |

3. Machine force calculations

The cost for machine force is calculated by using the following equation (I). By using the standardised write-down period of the UPV paper.

$$C_x = \frac{C_{eq} \cdot T_{use}}{P} \quad (I)$$

With:

C_x = write-down cost (€)

C_{eq} = total cost of equipment (€)

T_{use} = used time (months)

P = Write down period (months)

In Table 3 an estimation of the total cost for simulations is showed.

Table 3: Cost estimation for machine force

| Code | Description | Cost (€) | Price | | |
|---------------------------------|--------------------------------------------------------------------|----------|--------------------|-----------------|---------------|
| | | | Write-down (years) | Period (months) | Price (€) |
| MF 1 | Computers (2) | 2500.00 | 6 | 6 | 208.33 |
| MF 2 | Software Matlab R2020b | 800.00 | 6 | 4 | 44.44 |
| MF 3 | Microsoft Office 365 | 149.00 | 6 | 6 | 12.42 |
| MF 4 | Linux OS + KPP | Free | / | / | 0.00 |
| MF 5 | Meinhardt multifrequency laboratory reactor (500 mL) (subcontract) | 15000.00 | 12 | 1 | 104.17 |
| MF 6 | Huber Millichiller (subcontract) | 1000.00 | 12 | 1 | 6.94 |
| TOTAL MACHINE FORCE COST | | | | | 376.30 |

4. Subcontractors

The experiments were carried out by PhD E. Selva-Galvis. The workforce for the subcontractor is already included in Table 2. Beside the workforce, the used materials for the experiments are included in Table 3. Due to the low concentration of the pharmaceuticals, the cost of the pharmaceuticals is neglectable. One of the main operation costs for US treatment is the energy consumption of the transducers. The consumption is estimated 225 kWh. Also, the cost of each pharmaceutical analysis cannot be ignored. For each UHPLC analysis, an estimated cost of 10.50 euro is given. In the following lines, the estimated cost for the energy consumption and analysis will be made:

In total four experiments were carried out. One in short time (20 minutes), two including a pharmaceutical compound ACE or CIP (30 min) and one of 2.5 hours. The total energy cost is the price per kWh times the time of sonication and times the consumed energy. The energy price is calculated using the business electricity price from 2020. (https://www.globalpetrolprices.com/Spain/electricity_prices/)

Total time of use: 0.3 h + 2 x 0.5 h + 2.5 h = 3.8 hours

Total energy cost: 225 kWh x 3.8 h x 0.102 €/kWh = 82,20 €

For the cost of analysis is the cost for one analysis (10.50 €) times the number of analysis (NA). Each experiment, five samples were taken from the reactor for analysis.

NA = 2 x 5 = 10

Total cost of analysis: 10.50 €/Analysis x 10 analysis = 105.00 €

The total cost made by the subcontractor for energy and analysis is 187.20 €

5. Total cost

For the total cost of this work the indirect costs (which is 25 % of the sum of all the expenses) and the taxes (21 % of the total expenses) need to be taken into account.

| TOTAL COST CALCULATION | |
|--------------------------------|--------------------|
| Workforce cost | 12 537.00 € |
| Machine force cost | 376.30 € |
| Subcontractor cost | 187.20 € |
| Total cost of expenses | 13 100.50 € |
| Indirect costs (25 %) | 3 275.13 € |
| Total cost before taxes | 16 375.63 € |
| Taxes (21 %) | 3 438.88 € |
| Total cost after taxes | 19 814.51 € |

The total cost for this work was estimated on **16 375.50 €** before taxes, and **19 814.51 €** after taxes.

6. References

Electricity prices Spain, via https://www.globalpetrolprices.com/Spain/electricity_prices/, accessed on 16 July, 2021

http://www.upv.es/entidades/VIIT/menu_urlc.html?/entidades/VIIT/info/U0735197.pdf